

JGR Biogeosciences

RESEARCH ARTICLE

10.1029/2018JG004589

Key Points:

- The sensitivity of ecosystem carbon fluxes to root-zone soil moisture varies markedly across regions and vegetation types in North America
- Ecosystems with highest carbon flux moisture sensitivities are eastern deciduous forests, western conifer forests, and dryland grasslands
- Findings highlight the importance of improving terrestrial biosphere model predictions of regional soil moisture dynamics

Supporting Information:

- Supporting Information S1

Correspondence to:

K. Zhang and P. Moorcroft,
kzhang@hhu.edu.cn;
paul_moorcroft@harvard.edu

Citation:

Zhang, K., Ali, A., Antonarakis, A., Moghaddam, M., Saatchi, S., Tabatabaenejad, A., et al. (2019). The sensitivity of North American terrestrial carbon fluxes to spatial and temporal variation in soil moisture: An analysis using radar-derived estimates of root-zone soil moisture. *Journal of Geophysical Research: Biogeosciences*, 124, 3208–3231. <https://doi.org/10.1029/2018JG004589>






Received 18 MAY 2018

Accepted 23 AUG 2019

Accepted article online 8 OCT 2019

Published online 6 NOV 2019

The Sensitivity of North American Terrestrial Carbon Fluxes to Spatial and Temporal Variation in Soil Moisture: An Analysis Using Radar-Derived Estimates of Root-Zone Soil Moisture

Ke Zhang¹ , Ashehad Ali² , Alexander Antonarakis³, Mahta Moghaddam⁴, Sassan Saatchi⁵, Alireza Tabatabaenejad⁴ , Richard Chen⁴, Sermak Jaruwatanadilok⁵, Richard Cuenca⁶, Wade T. Crow⁷ , and Paul Moorcroft² 

¹State Key Laboratory of Hydrology-Water Resources and Hydraulic Engineering, and College of Hydrology and Water Resources, Hohai University, Nanjing, China, ²Department of Organismic and Evolutionary Biology, Harvard University, Cambridge, MA, USA, ³Department of Geography, University of Sussex, Brighton, UK, ⁴Ming Hsieh Department of Electrical Engineering/Electrophysics, University of Southern California, Los Angeles, CA, USA, ⁵Jet Propulsion Laboratory, California Institute of Technology, Pasadena, CA, USA, ⁶Department of Biological and Ecological Engineering, Oregon State University, Corvallis, OR, USA, ⁷ARS Hydrology and Remote Sensing Laboratory, United States Department of Agriculture, Beltsville, MD, USA

Abstract This study examines the impact of variation in root-zone soil moisture (RZSM), a key component of the Earth's hydrologic cycle and climate system, on regional carbon fluxes across seven North American ecosystems. P-band synthetic aperture radar-derived RZSM estimates were incorporated into the ecosystem demography (ED2) terrestrial biosphere model through a model-data blending approach. Analysis shows that the model qualitatively captures inter-daily and seasonal variability of observed RZSM at seven flux tower sites ($r = 0.59 \pm 0.26$ and $r = 0.70 \pm 0.22$ for 0–10 and 10–40 cm of soil layers, respectively; $P < 0.001$). Incorporating the remotely sensed RZSM estimates increases the accuracy (root-mean-square deviations decrease from 0.10 ± 0.07 and $0.09 \pm 0.06 \text{ m}^3 \cdot \text{m}^{-3}$ to 0.08 ± 0.05 and $0.07 \pm 0.03 \text{ m}^3 \cdot \text{m}^{-3}$ for 0–10 and 10–40 cm of soil layers, respectively) of the model's RZSM predictions. The regional carbon fluxes predicted by the native and RZSM-constrained model were used to quantify sensitivities of gross primary productivity, autotrophic respiration (R_a), heterotrophic respiration (R_h), and net ecosystem exchange to variation in RZSM. Gross primary productivity exhibited the largest sensitivity ($6.6 \pm 10.7 \text{ kg} \cdot \text{cm}^{-2} \cdot \text{year} \cdot \theta^{-1}$) followed by R_a ($2.9 \pm 7.3 \text{ kg} \cdot \text{cm}^{-2} \cdot \text{year} \cdot \theta^{-1}$), R_h ($2.6 \pm 3.1 \text{ kg} \cdot \text{cm}^{-2} \cdot \text{year} \cdot \theta^{-1}$), and net ecosystem exchange ($-1.7 \pm 7.8 \text{ kg} \cdot \text{cm}^{-2} \cdot \text{year} \cdot \theta^{-1}$). Analysis shows that these carbon flux sensitivities varied considerably across regions, reflecting influences of canopy structure, soil properties, and the ecophysiological properties of different plant functional types. This study highlights (1) the importance of improved terrestrial biosphere model predictions of RZSM to improve predictions of terrestrial carbon fluxes, (2) a need for improved pedotransfer functions, and (3) improved understanding of how soil characteristics, climate, and vegetation composition interact to govern the responses of different ecosystems to changing hydrological conditions.

1. Introduction

Soil moisture is a key variable of the earth system influencing terrestrial water, carbon and nutrient cycling, and the exchange of carbon, water, and energy between the land-surface and atmosphere. In particular, it impacts meteorological, hydrological, and ecological processes and properties including surface energy balance (Berg et al., 2014; Ford et al., 2015; Gallego-Elvira et al., 2016; Lin & Cheng, 2016; Suarez et al., 2014), land surface albedo (Liu et al., 2014; Zhang et al., 2014), soil thermal properties (Juszak et al., 2016; Sugathan et al., 2014), runoff (Crow & Ryu, 2009; Morbidelli et al., 2016), plant water stress (He et al., 2016), and resulting vegetation productivity and ecosystem carbon fluxes (Huang et al., 2016; Jia et al., 2016; McInerney & Helton, 2016; Xu et al., 2004; Xu & Zhou, 2005).

Improved measurements of spatial and temporal patterns of variation in soil moisture are therefore essential for improved characterization of meteorological, hydrological, and ecological processes for

hydrological forecasting, weather prediction, and estimates of terrestrial carbon, water, and energy fluxes. Traditionally, soil moisture has been measured through ground-based instruments that provide accurate, high temporal resolution information about the dynamics of soil moisture at specific locations; however, measurements from ground-based observations are limited in their spatial extent (Dorigo et al., 2011). Satellite remote sensing of soil moisture is an alternative approach that can be used to provide spatially-comprehensive measurements of soil moisture, albeit with reduced spatial and temporal resolution compared to ground-based sensors. Numerous satellite-based active and passive microwave sensors launched since 1970s have been widely used to estimate regional and global near-surface soil moisture, including Scanning Multichannel Microwave Radiometer (Paloscia et al., 2001), Advanced Microwave Scanning Radiometer on the Earth Observing System (Njoku et al., 2003), the Soil Moisture and Ocean Salinity Sensor (Kerr et al., 2012), the Advanced Scatterometer (Lindell & Long, 2016), the Fengyun Satellites (Parinussa et al., 2014; Song & Jia, 2016), the Advanced Microwave Scanning Radiometer 2 (Parinussa et al., 2015), and the Soil Moisture Active Passive (Entekhabi et al., 2010). Recently, navigation signals from global navigation satellite systems have also been utilized to retrieve soil moisture (Camps et al., 2016; Kim & Lakshmi, 2018). Though the technology to retrieve soil moisture profile from spaceborne scatterometer has been developed (Wagner et al., 1999), current satellite retrievals of soil moisture only routinely provide estimates of near-surface soil moisture, *i.e.* soil moisture in the top few centimeters of soil.

The National Aeronautics and Space Administration (NASA) Earth Ventures 1 Airborne Microwave Observatory of Subcanopy and Subsurface (AirMOSS; <https://airmoss.jpl.nasa.gov/>) is a new airborne P-band synthetic aperture radar (SAR) designed to provide direct retrievals of root-zone soil moisture (RZSM) up to 120 cm in depth (depth of penetration varies depending on the amount of vegetation cover) using active remote sensing (Tabatabaenejad et al., 2015). As its name implies, RZSM is a critical soil moisture state variable that influences plant functioning, including photosynthesis (Xia et al., 2017), ecosystem respiration (Flanagan & Johnson, 2005), and soil respiration (Ito & Ishida, 2016).

Accurate characterization of RZSM in land surface models, terrestrial biosphere models, and earth system models is critical for accurately estimating short-term (hourly-yearly), medium-term (yearly-to-decadal), and long-term (decadal-to-centennial) carbon, water, and energy fluxes. With regard to water fluxes, previous studies have shown that there are model-dependent, systematic biases in model-based estimates of soil moisture or RZSM when against ground observations (Koster et al., 2009; Loew et al., 2013; Pan et al., 2016; Verrot & Destouni, 2016; Xia et al., 2014) and remotely sensed measurements of near-surface soil moisture (Gumuzzio et al., 2016; Polcher et al., 2016), and that models show divergent biases (van den Hurk et al., 2016). With respect to carbon fluxes, Kim et al. (2015) demonstrated the importance of soil moisture stress response functions for predictions of carbon fluxes in the Ent Terrestrial Biosphere Model. In addition, two recent studies have examined the sensitivities of soil carbon flux predictions to soil moisture at the global scale. Exbrayat et al. (2013) implemented three different functions describing how soil moisture affected carbon decomposition rates within the Community Atmosphere Biosphere Land Exchange land surface model coupled with the Carnegie-Ames-Stanford Approach Carbon-Nitrogen-Phosphorus land biogeochemical model, and showed that its predictions of soil carbon stocks varied significantly depending on the functional form chosen. Hursh et al. (2017) analyzed the sensitivity of soil respiration measurements to soil moisture and showed that, although soil temperature is the dominant driver of global scale variation in soil respiration fluxes, within certain biomes, soil moisture is the dominant predictor of variation in soil respiration fluxes.

In this study, we use the AirMOSS measurements of RZSM (0–100 cm) collected in luation regions spanning five North American biomes, in conjunction with a terrestrial biosphere model, to examine the relationship between spatial variation in RZSM and spatial variability in terrestrial carbon fluxes. Using a simple, but effective, model-data blending method (described in section 2.3) to assimilate the three-dimensional AirMOSS RZSM products into the terrestrial biosphere model we produced AirMOSS-constrained predictions of terrestrial carbon fluxes for the seven evaluation regions. We then used the RZSM measurements and model predictions of resulting carbon fluxes to quantify the impact of spatial and temporal variation in RZSM on the estimation of regional-scale carbon fluxes.

2. Materials and Methods

2.1. Study Areas

The evaluation regions are seven areas of approximately 2,500 km² surrounding seven FLUXNET tower sites within the contiguous United States that were surveyed by the AirMOSS project from 2012 to 2015 (Tabatabaenejad et al., 2015; Figure 1). The Howland Forest, Harvard Forest, Duke Forest, Metolius, Tonzi Ranch, and Walnut Gulch evaluation regions are all rectangular, 100 km × 25 km areas, while the Marena In Situ Sensor Testbed (MOISST) site in Oklahoma is of a similar size, but has a more complex geometry. Each evaluation region includes a corresponding FLUXNET tower site, specifically, the Howland Forest main tower (USHo1; Hollinger et al., 2004), the Harvard Forest EMS tower (USHa1; Urbanski et al., 2007), the Duke Forest loblolly pine site (USDk3; Palmroth et al., 2005), the Metolius intermediate pine site (USMe2; Thomas et al., 2009), the Tonzi Ranch site (USTon; Baldocchi et al., 2004), the Walnut Gulch Kendall Grasslands site (USWkg; Scott, 2010), and the Atmospheric Radiation Measurement Southern Great Plains site (USARM) located within the MOISST evaluation region (Lokupitiya et al., 2009).

The seven evaluation regions span five North American biomes: temperate broadleaf and mixed forests (Howland Forest, Harvard Forest, and Duke Forest); temperate conifer forests (Metolius); temperate grasslands and croplands (MOISST); Mediterranean forest, woodlands, and scrub (Tonzi Ranch); and deserts and xeric shrublands (Walnut Gulch; Figure 1 and Table 1). To compare the composition of these regions, we examined the fractions of land cover types obtained from the 30-m National Land Cover Database (NLCD 2011) map (Homer et al., 2015), and computed the percentage contribution of each plant functional type (PFT) to the total canopy leaf area index (LAI) within each region. Representative species of each PFT are given in Table 2, and details the LAI calculation can be found in section 2.5 of the manuscript. The Howland, Harvard, and Duke Forest regions were all classified as temperate broadleaf and mixed forest; however, the land cover and PFT composition of their plant canopies differ: the Howland Forest region is primarily mixed temperate forest (29.2%), evergreen needleleaf forest (24.5%), and deciduous broadleaf forest (16.4%) with late-successional conifer and middle-successional hardwoods as the dominant PFTs (51.4% and 16.9%, respectively); the Harvard Forest region is primarily deciduous broadleaf forest (30.8%), mixed temperate forest (22.0%), and evergreen needleleaf forest (22.0%) with mid-successional hardwoods and northern pines as the dominant PFTs (40.4% and 20.0%, respectively); the Duke Forest region is primarily deciduous broadleaf forest (43.2%) and mixed forest (14.2%) with middle-successional hardwoods and southern pines as the dominant PFTs (38.8% and 26.9%, respectively). The Metolius region is primarily evergreen needleleaf forest (55.2%) and shrubland (31.6%), the former being found mainly in the western part, and the latter being found mainly in the eastern portion of the region see (Figure 1) with firs and western pines as the dominant tree PFTs (71.3% and 26.2%, respectively). The Tonzi Ranch region is primarily grasslands (46.3%) and shrublands (21.1%) with dryland C₃ grass, western pines, and western hardwoods as the dominant PFTs (40.5%, 30.3%, and 21.9%, respectively). The MOISST region is primarily grasslands (44.0%) and croplands (38.3%) with C₃ crops and dryland C₄ grasses as the dominant PFTs (34.7% and 29.8%, respectively). In contrast to the above six regions, the Walnut Gulch region has a relatively homogeneous land cover, being primarily shrubland (87.2%) with dryland C₄ grass and northern pine as the dominant PFTs (68.3% and 17.2%, respectively). As Figure 1 illustrates, these seven regions span a large range of biomes, land cover types, and PFT compositions found across North America.

2.2. ED2 Terrestrial Biosphere Model

The terrestrial biosphere model used in this study is the ecosystem demography model version 2 (ED2), an integrated terrestrial biosphere model incorporating hydrology, land-surface biophysics, vegetation dynamics, and soil carbon and nitrogen biogeochemistry (Medvigy et al., 2009). Like its predecessor, ED (Hurtt et al., 1998; Moorcroft et al., 2001), ED2 tracks the changing abundance of plants of different sizes and PFTs arising from plant growth, mortality, recruitment, and the impact of disturbances using a set of size- and age-structured partial differential equations. The size- and age-structured PDEs are initialized with an initial condition corresponding to the initial size and age distributions of the PFTs at the beginning of the simulation. Previous studies have shown that ED2 is able to realistically represent the dynamics of vertically resolved and spatially heterogeneous plant communities incorporating the effects of natural disturbance processes such as fire, and anthropogenic disturbances such as forest harvesting or land clearing (e.g., Albani et al., 2006; Hurtt et al., 2004; Medvigy et al., 2009). We used a version branched from the latest ED2

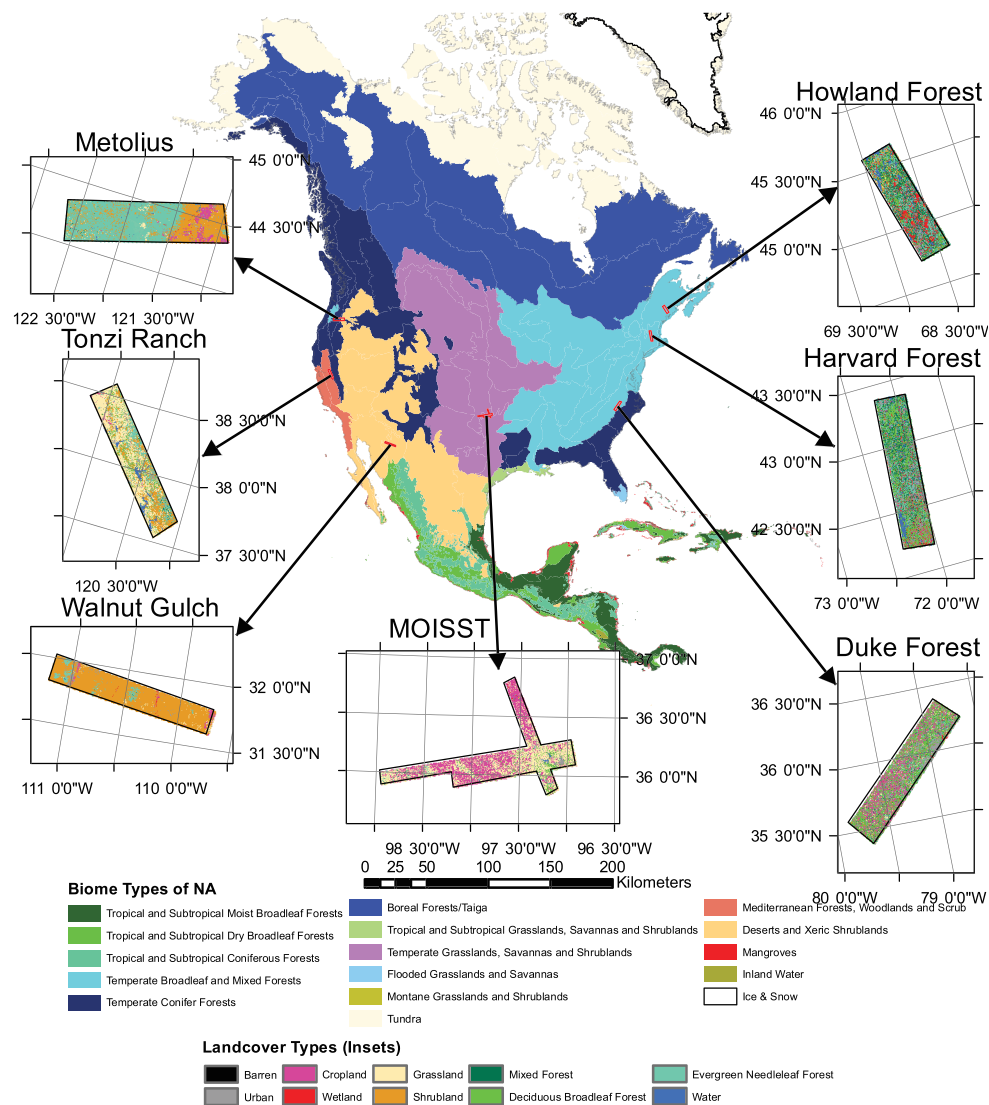


Figure 1. Biomes in North America, and locations and NLCD land cover maps of the seven study areas.

Table 1

Percentage Abundances (%) of the Different Plant Functional Types Across the Seven Evaluation Regions

		Plant functional types												
Region	Biome types	EHW	MHW	LHW	WHW	NP	LC	SP	WP	FR	DC3	DC4	CRC3	CRC4
Howland	Temperate broadleaf and mixed forest	11.5	16.9	12.6	—	7.5	51.4	—	—	—	—	—	0.1	—
Harvard	Temperate broadleaf and mixed forest	9.0	40.4	14.3	—	20.0	16.2	—	—	—	—	—	0.1	—
Duke	Temperate broadleaf and mixed forest	10.0	38.8	7.3	—	—	—	26.9	—	—	0.3	—	16.8	—
Metolius	Temperate conifer forest	0.1	—	0.2	0.6	0.1	—	—	26.2	71.3	1.2	—	0.3	—
Tonzi	Mediterranean forest, woodland, and scrub	1.7	—	0.2	21.9	—	—	—	30.3	5.2	40.5	—	0.2	—
Walnut	Deserts and xeric shrublands	1.5	—	—	—	17.2	—	—	9.4	0.6	—	68.3	3.0	—
MOISST	Temperate grasslands and croplands	7.7	21.0	0.7	—	—	—	3.8	—	—	2.3	29.8	33.3	1.4

Note. Abundance values reflect the percentage of the total LAI within each region. Details on this calculation can be found in section 2.5. CRC3 = C₃ crop; CRC4 = C₄ crop; DC3 = dryland C₃ grass; DC4 = dryland C₄ grass; EHW = early-successional hardwood; FR = fir; LAI = leaf area index; LC = late-successional conifer; LHW = late-successional hardwood; MHW = middle-successional hardwood; NP = northern pine; SP = southern pine; WHW = western hardwood; and WP = western pine.

Table 2

Plant Functional Types (PFTs) Implemented in the ED2 Model Analysis Used in This Study, and Representative Plant Species

PFTs	Representative species
Northern pine	<i>Pinus resinosa</i> and <i>Pinus strobus</i>
Southern pine	<i>Pinus taeda</i> , <i>Pinus strobiformis</i> , and <i>Pinus palustris</i>
Later-successional conifer	<i>Thuja occidentalis</i> , <i>Picea rubens</i> , <i>Picea glauca</i> , <i>Tsuga canadensis</i> , and <i>Abies balsamea</i>
Early-successional hardwood	<i>Betula papyrifera</i> , <i>Betula populifolia</i> , <i>Betula lenta</i> , and <i>Prunus</i> spp.
Middle-successional hardwood	<i>Quercus rubra</i> , <i>Quercus velutina</i> , <i>Acer rubrum</i> , <i>Fraxinus americana</i> , and <i>Sorbus americana</i>
Late-successional hardwood	<i>Acer saccharum</i> , <i>Fagus grandifolia</i> , <i>Betula alleghaniensis</i>
C ₃ crop	<i>Triticum astivum</i> , <i>Triticum militinae</i> , <i>Triticum monococcum</i> , <i>Triticum spelta</i> , <i>Glycine max</i>
C ₄ crop	<i>Zea mays</i> , <i>Sorghum bicolor</i>
Western hardwood	<i>Quercus kelloggii</i> , <i>Quercus engelmannii</i> , <i>Quercus agrifolia</i> , <i>Quercus lobata</i>
Western pine	<i>Pinus ponderosa</i> , <i>Pinus monticola</i> , <i>Pinus edulis</i> , <i>Sequoiadendron giganteum</i>
Fir	<i>Abies amabilis</i> , <i>Abies concolor</i> , <i>Abies magnifica</i> , <i>Abies grandis</i> , and <i>Pseudotsuga menziesii</i>
Dryland C ₄ grass	<i>Erograstis lehmanniana</i> , <i>Bouteloua</i> spp., and <i>Sorghum halepense</i>
Dryland C ₃ grass	<i>Brachypodium distachyon</i> , <i>Hypochaeris glabra</i> , and <i>Trifolium hirtum</i>

github repository (Rev-84, <https://github.com/EDmodel/ED2>; Knox, 2012; Longo, 2014) to conduct the model simulations. The source code used in this study can be downloaded from <https://moorcroftlab.oeb.harvard.edu/code-data>. The latest ED2 version incorporates comprehensive biophysical and biogeochemical modules that solve the coupled energy, water, and carbon budgets of the plants within the canopy at sub-daily scale. This model accounts for important effects of day-to-day and within-day variability, and competition for light and water over heterogeneous landscapes. In terms of soil moisture dynamics, ED2 uses a generalized version of the Land Ecosystem Atmosphere Feedback-2 (LEAF 2) soil moisture scheme (Walko et al., 2000), which has a multilayer soil column and is able to represent liquid or frozen surface water both in and above the soil. Soil moisture movement between soil layers is governed by moisture potential gradient through Darcy's law. ED2 has been used to study a number of terrestrial ecosystem processes including: the hydrometeorological effects of land conversion on ecosystems (Knox et al., 2015), the response of Amazon ecosystems to climate and land-use change (Zhang et al., 2015), and to quantify resilience of the Amazon to climate change, (Levine et al., 2016).

In this study, we conducted model simulations at both site and regional scales. Site-level simulations at the seven flux tower sites used initial conditions and meteorological forcing specified from measurements: The simulations were driven by observed site-level meteorological data, used site-level soil texture and depth information, and the ecosystem composition and structure at each site was specified from ground inventory measurements. In the regional-level simulations, 13 PFTs (four hardwood trees, five conifer trees, C₃ and C₄ grasses, and C₃ and C₄ crops) were used to represent the plants across the seven study regions. The list of PFTs used in the simulations and their representative plants species are listed in Table 2. The western hardwood, western pine, fir, and dryland C₄ grass, and dryland C₃ grass PFTs are the new PFTs implemented in the ED2 model and were parameterized in this study. To obtain the optimized ecophysiological and life-history parameters for the five new PFTs in the ED2 model, we applied the standard Markov chain Monte Carlo (MCMC) method (Gelman & Rubin, 1992) to approximate the posterior distributions of these parameters. The final parameter values are set as the means of their posterior distributions. The MCMC method was applied to derive the posterior parameter values of western hardwood and dryland C₃ grass, western pine and fir, and dryland C₄ grass through site-level MCMC simulations at the USTon, USMe2, and USWkg sites, respectively. The data constrains include hourly, monthly, and yearly net ecosystem exchange (NEE; both daytime and nighttime), heat fluxes (latent and sensible heats), and site-specific multilayer soil water contents from tower measurements, changes in basal area from tower ground census, and daily LAIs from the Moderate Resolution Imaging Spectroradiometer (MODIS) Collection 6 record (Yan et al., 2016). The methods used to derive initial conditions for the regional simulations are described in section 2.5.

The simulations for each region were conducted on a 30 arc-second (about 1 km) grid resolution. This resolution was chosen to achieve a balance between high spatial resolution and manageable model computational load. For spatial consistency, the vertical soil profile in each pixel was represented as a series of stacked layers with the following thicknesses: 0–2, 2–8, 8–20, 20–40, 40–80, 80–160, 160–300, 300–500, and 500–800 cm. The number of soil layers present within a given grid cell was determined by the depth data

from the measurement-based soils data set (see section 3). The biogeophysical and biogeochemical processes were solved using a fourth-order Runge-Kutta integration scheme with an integration time step of 600 s with hourly outputs of the relevant state variables and fluxes.

2.3. AirMOSS L2/3 RZSM and its Incorporation into ED2

The NASA AirMOSS mission used an airborne ultra-high frequency P-band SAR onboard a Gulfstream-III aircraft to measure RZSM (Chapin et al., 2012; <https://airmoss.jpl.nasa.gov/>). In contrast to previous remote-sensing estimates of soil moisture, the AirMOSS P-band SAR has the capability to penetrate through vegetation canopies down to soil depths of approximately 1.2 m, the extent of the penetration varying depending on soil wetness, soil type, and vegetation type (Chapin et al., 2012; Tabatabaenejad et al., 2015). Two algorithms were used to estimate RZSM from the raw radar backscatter measurements: A numerical radar scattering model was used to estimate RZSM from the P-band SAR data over the shrubland, sparsely vegetated regions, and locations where the land cover has a predominance of a single woody species (Tonzi Ranch, Walnut Gulch, MOISST, and Metolius; Tabatabaenejad et al., 2015), while a simplified 3-D model of forest canopy was used to estimate RZSM over the more compositionally-diverse forested regions of Howland, Harvard, and Duke (Truong-Loi et al., 2015). In both cases, the vertical profile of soil moisture was estimated using a second-order polynomial representation of the profile. The AirMOSS Level 2/3 RZSM data, hereafter referred to as L2/3 RZSM, provided vertically resolved estimates of RZSM down to 100-cm depth at a spatial resolution of 3 arc-seconds <https://doi.org/10.3334/ORNLDAAAC/1418>. The 3 arc-second measurements were then aggregated to 30 arc-second ED2 simulation grids. The temporal resolution of the RZSM data over each site is sufficiently high (all values taken within an interval of less than 1 hr), and thus each aggregated L2/3 RZSM data set essentially provides a snapshot of soil moisture over each region.

The L2/3 RZSM measurements provide opportunistic snapshots of spatial patterns of RZSM, in which the time intervals between successive snapshots range from a few days to several months. Since these observation intervals are larger than the typical response time of ED2 soil moisture, conventional data assimilation approaches such as an ensemble Kalman filter will simply relax back to background model predictions in the lengthy interval between observations, thus negating the impact of the L2/3 RZSM assimilation (Walker & Houser, 2004).

Accordingly, in this study, we developed a simple assimilation methodology to utilize the temporally infrequent L2/3 RZSM ($\theta_{L2/3}$) to correct the hourly ED2 RZSM predictions on each grid cell-by-cell basis to produce a blended hourly RZSM series. First, a conventional ED2 simulation was run to produce hourly multilayer (maximum nine layers) gridded predictions of ED2 RZSM (θ_{ED}) across each region. Second, for each grid cell, we then estimated the bias (ϵ) in the model's predictions by treating $\theta_{L2/3}$ at the same soil layer as a more accurate estimate and computing ϵ as a difference between θ_{ED} and $\theta_{L2/3}$ (i.e., $\epsilon = \theta_{ED} - \theta_{L2/3}$). The bias values for each grid cell were then linearly interpolated into hourly values, which were then subtracted from θ_{ED} to produce a bias-reduced blended RZSM estimate that we referred to as L2/3 RZSM-B (Supporting Information, Figure S1). To ensure physical consistency, the bias reduction method also took into account the physical bounds of maximum and minimum water content of the soil (i.e., saturated soil water content and residual soil water content), which was calculated based on the soil type of each grid cell. Finally, we used the multilayer L2/3 RZSM-B as prescribed RZSM values for the ED2 model to rerun it to simulate the carbon fluxes.

2.4. Quantification of Carbon Flux Sensitivities to RZSM

Similar to the carbon sensitivity metric of Friedlingstein et al. (2006), we defined a set of sensitivity factors to quantify the sensitivities of predicted carbon fluxes to variation in RZSM (θ , 0–100 cm):

$$\beta_C = \frac{C_{ED}(\theta_{ED}) - C_{ED}(\theta_{RZSM})}{\theta_{ED} - \theta_{RZSM}}, \quad (1)$$

where $C_{ED}(\theta)$ denotes a given carbon flux (gross primary productivity [GPP], autotrophic respiration [R_a], heterotrophic respiration [R_h], ecosystem respiration [R_{eco}], or net ecosystem exchange [NEE]; θ_{ED} is the RZSM predicted by the ED2 model; θ_{RZSM} is either observed RZSM or L2/3 RZSM-B; $C_{ED}(\theta_{ED})$ is the original modeled carbon flux and $C_{ED}(\theta_{RZSM})$ is the carbon flux predicted by the model when the by RZSM values are

either prescribed from observations or from the L2/3 RZSM-B; and β_C is the carbon flux sensitivity factor. Essentially, the β_C value quantifies the predicted response of a given carbon flux to change in RZSM with the magnitude of the change reflecting the difference between the predicted and estimated observed value of RZSM: Higher absolute values of β_C indicate higher sensitivity of the carbon fluxes to changes in RZSM while the sign indicates the direction of the carbon flux (positive values indicating a flux to the atmosphere and negative values indicating net carbon uptake by the ecosystem).

2.5. Model Initialization

The aboveground ecosystem composition is described in terms of initial abundances of individuals of different sizes and different PFTs within the grid cells of each evaluation region. This ecosystem composition and structure information was derived by combining information about the fractional coverage of bare ground, grassland, croplands, and forest within each 30" (~1 km) grid cell specified from the 30-m NLCD data set (Homer et al., 2015) with information about the size and abundances of the eight different tree PFTs specified from forest inventory data from the U.S. Forest Service's Forest Inventory and Analysis (FIA) program (McRoberts et al., 2005; Shaw, 2009). Specifically, the NLCD 2011 with a spatial resolution of 30 m (Homer et al., 2015) was first used to calculate the fractional coverage of bare ground, grassland, croplands, and forest/woodlands within each 30" (~1 km) grid cell of the radar swath (Figure 1). In areas dominated by grasslands and croplands, the abundances of the grass and crop PFTs were then calculated from the seasonal maximum LAI derived from the 2002–2014 MODIS Collection 6 record (Yan et al., 2016) using ED2's definition of a PFT's ecophysiological properties and specific leaf area (Table S1). For the forested fraction of each grid cell, the initial forest structure and composition was determined from the subplots of nearest three FIA plots. The density of FIA plots can vary by region and state and can be ~3–6 plots per 10 km² on average for eastern and western areas and ~1.5 plots per 10 km² in the midwest. While this procedure means that some adjacent grid cells may have the same individual tree information and consequently the forested fractions of such grid cells will have identical canopy structure and composition, the grid cells will differ in their forested fractions. The most recent FIA census in the FIA's 1999–2011 data set were used to specify the fine-scale spatial heterogeneity in the structure and composition of the plant canopy following the methodology of Medvigy and Moorcroft (2012) in which the FIA data are used to prescribe the diameters at breast height (cm), and the species identity of each stem is assigned to the closest of the nine tree PFTs listed in Table 2. The estimates of abundances for each PFT found in Table 1 were calculated from these aboveground ecosystem composition estimates within each grid cell by calculating the percentage contribution of each PFT to the total canopy LAI within each region.

The initial values of the soil organic carbon were extracted from FIA plot values of carbon in the litter pool and carbon in the soil organic material, with values converted from tons per acre to kilograms per square meter. Fast soil carbon and structural soil carbon in the ED2 model are extracted from the litter pool and soil organic material pool, respectively. Because there is no data in the FIA database for the slow soil carbon pool, initial slow soil carbon values were estimated from a simulation of the model initialized with the FIA-derived ecosystem composition driven by recycling 2009–2014 North American Land Data Assimilation Version 2 (NLDAS-2) meteorological forcings (Xia et al., 2012). For the regional simulations, the ED2 model was started with the simulation in 2010 with the aforementioned initial conditions and driven by the 2009–2014 NLDAS-2 meteorological forcing.

In the site-level simulations, the aboveground ecosystem composition is derived from censuses conducted at the flux tower sites using the data from census that was conducted closest to 2010, the start of the simulation period. The initial values of the soil organic carbon were extracted from the flux tower reported values. The soil text, soil depth, and meteorological data were also derived by the ground measurements from the AmeriFlux network (<http://ameriflux.lbl.gov>). Since USDk3 was terminated in 2008, the meteorological forcings at this site were specified from the NLDAS-2 data set.

2.6. Model Evaluation

The model performance is evaluated using the following procedures. First, we compared the modeled RZSM, AirMOSS L2/3 RZSM, and ground-measured RZSM from the AirMOSS L2 hourly in-ground soil moisture observations (https://daac.ornl.gov/AIRMOSS/guides/AirMOSS_L2_Inground_Soil_Moist.html) in two soil layers (0–10 and 10–40 cm) from 2012 to 2013 at the seven flux tower sites. Second, we compared the spatial

patterns of the model and AirMOSS L2/3 RZSM across the seven evaluation regions. Furthermore, we evaluated the modeled carbon flux (C-flux) sensitivities to RZSM by a comparison with their observation-based counterparts, which are derived from the tower measured C-flux data from 2010 to 2014 provided by the AmeriFlux network (<http://ameriflux.lbl.gov>) at six flux tower sites (USDk3 was terminated in 2008 and is excluded from this analysis). Because there are no direct observations of the C-flux sensitivities to RZSM at the seven flower towers, we used the measurement-based daily carbon fluxes from 2010 to 2014 from six of the seven flux towers to derive measurement-based C-flux sensitivities. We then compared the modeled C-flux sensitivities to RZSM with the measurement-derived values. Since no data was available from experimental RZSM manipulations at the seven sites, we estimated the observed soil moisture sensitivities by daily differencing carbon flux and soil moisture measurements from two consecutive days during which meteorological conditions did not change substantially, defined by two conditions: (1) the absolute relative difference of daily air temperature and daily incoming shortwave radiation between the two days are less than or equal to 10%, and (2) absolute relative difference of daily precipitation between the 2 days are less than or equal to 11 mm.

To measure the quality of model predictions, three statistical metrics were used: Pearson's correlation coefficient, root mean squared error (RMSE), and bias (model minus observation).

2.7. Attribution of Spatial Variability in Model RZSM Biases and C-flux Sensitivities

We used a multiple linear regression analysis to investigate the relationships between the carbon flux sensitivities and potential controlling factors, including aboveground biomass (AGB), LAI, soil carbon storage, sand percentage, clay percentage, and PFT (the later as a categorical variable). We also applied an analysis of variance (ANOVA) analysis to test the difference of the C-flux sensitivities among PFTs. The multiple linear regression was conducted using the linear model function (`lm`), and the one-way ANOVA analysis was conducted using the pairwise *t*-test function (`pairwise.t.test`), both in R 3.4.1 (<https://www.r-project.org>).

In addition, sensitivity analyses of model RZSM and carbon fluxes (GPP, ecosystem respiration and NEE) on soil texture (sand and clay percentages) at the seven flux tower sites were conducted to estimate the impacts of uncertainty in soil texture data on the model estimates of RZSM and carbon fluxes.

3. Data

3.1. Soil Data

The soil physical and hydraulic properties were obtained from the gridded Soil Survey Geographic Database (gSSURGO; <https://websoilsurvey.nrcs.usda.gov/>, access date: 2012) in conjunction with Rosetta, a computer program for estimating soil hydraulic parameters with hierarchical pedotransfer functions (<http://www.cals.arizona.edu/research/rosetta/index.html>). The soil physical and hydraulic properties required by the ED2 biosphere model include fractions of sand, clay and silt, soil class, soil stratification (soil layers and depths), saturated soil water content (θ_s), and residual soil water content (θ_r). The lower soil boundary condition is also derived from the SSURGO (Soil Survey Geographic Database) data set. In addition, the SSURGO data set also provides the soil depth information, which is used to determine the number of soil layers in each modeling grid cell.

3.2. Land Cover/Land Use and Phenology Data

The land cover/land use was specified from the NLCD 2011 data set with a spatial resolution of 30 m (<https://www.mrlc.gov/data/nlcd-2011-land-cover-conus>). As described in section 2.5 above, these data, in combination with FIA measurements, were used to prescribe ecosystem structure and composition within each grid cell. Phenology was determined from the MODIS Global Land Cover Dynamics (MCD12Q2) Version 6 data product for the 2009–2014 period (<https://e4ftl01.cr.usgs.gov/MOTA/MCD12Q2.006/>; Ganguly et al., 2010), which was used to determine the timing of leaf onset and offset for the deciduous tree PFTs in the ED2 model.

3.3. Meteorological Forcing Data

The meteorological inputs were comprised of hourly time series of over-canopy air temperature, downward shortwave and longwave radiation, precipitation, specific humidity, wind velocities, and surface air pressure. These data are obtained from the NLDAS-2 (Xia et al., 2012) forcing data set. Because NLDAS-2 has a coarser

spatial resolution ($1/8^\circ \times 1/8^\circ$) than the $30''$ resolution of the regional simulation grids, bilinear interpolation was applied to downscale the data set to the spatial resolution of the regional simulation grids. In addition, atmospheric CO_2 concentration was specified from the NOAA GLOBALVIEW product (<https://www.esrl.noaa.gov/gmd/ccgg/globalview>).

4. Results

4.1. Evaluation of Soil Moisture Predictions and Blending Procedure

The ED2 RZSM predictions and AirMOSS-derived L2/3 RZSM-B estimates for 0–10 and 10–40 cm of soil layers were compared to in-situ soil moisture observations at the seven flux tower sites (Figure 2). Comparing the model's RZSM predictions against the *in-situ* observations shows that the native ED2 model qualitatively captures inter-daily and seasonal variability of observed RZSM between March 2012 and August 2014 across the seven flux tower sites (mean Pearson's correlation coefficient, $r = 0.59 \pm 0.26$ and $r = 0.70 \pm 0.22$ for the 0–10 and 10–40 cm of soil layers, respectively; sample sizes given by the value of n_{obs} in each panel of the figure, $P < 0.001$). ED2 RZSM performs best at Metolius (USMe2), Walnut Gulch (USWkg), and the 0- to 10-cm layer at Tonzi Ranch (USTon; Figure 2). The site-level correlation coefficients between ED2 RZSM and in situ observations at these three sites range from 0.75 to 0.88 ($P < 0.001$), with root mean square (RMSEs) between ED2 RZSM and the observations between 0.03 and 0.09 m^3/m^3 , and biases (model minus observation) between -0.02 and $0.04 \text{ m}^3/\text{m}^3$ (see Table S2). The correlation coefficients (r) between the model and observations for the 0–10 and 10–40 cm of layers at Duke Forest and for the 10- to 40-cm layer at Tonzi are also relatively high ($r = 0.7$, 0.73 and 0.88 respectively; $P < 0.001$); however, the model exhibits a significant dry bias in its predictions for these layers (biases of -0.12 , -0.14 and -0.18 respectively, see Table S2). At Howland (USHo1), the model predictions correlate moderately well with the observations in the upper soil layer and well in the 10–40 cm layer ($r = 0.57$ and 0.82 , respectively; $P < 0.001$), but with significant wet biases (biases of 0.22 and 0.16 respectively, see Table S2). At Harvard (USHa1), the model performs poorly in the 0- to 10-cm soil layer ($r = 0.2$; $P < 0.001$), performs well ($r = 0.82$; $P < 0.001$) in the 10- to 40-cm soil layer, but has a significant dry bias in both layers (Table S2). At the MOISST (USARM) site, the model performs poorly in both layers ($r = 0.25$ and 0.21 for the 0–10 and 10–40 cm of layers, respectively; $P < 0.001$), albeit with low overall bias (0.03 and -0.008 respectively, see Table S2). Taken together, these results suggest that the ED2 model is generally able to capture inter-daily and seasonal patterns of variability of RZSM across the seven sites that have different climate, soil, and ecosystem composition; however, there are still significant, unaccounted for, biases in the ED2 RZSM predictions at several of the sites.

Comparison of the ED2 RZSM predictions and L2/3 RZSM estimates to the ground observations across the seven sites (see Figure 2 and Text S1) for times which all three estimates are available (i.e., times that coincident with the red points in Figure 2) indicates that the L2/3 measurements are generally closer to the ground observations than the ED2 predictions in both soil layers (correlation coefficients $r = 0.64$ and 0.67 for the L2/3 RZSM vs. $r = 0.30$ and 0.31 for the ED2 RZSM predictions in the 0–10 and 10–40 cm of soil layers, respectively, sample size $n_{2/3} = 101$). The higher accuracy of the SAR-retrieved RZSM estimates compared to the native ED2 RZSM predictions justifies the incorporation of the L2/3 RZSM estimates into the ED2 model.

Following the application of the soil moisture blending method (section 2.3 and Figure S1), the blended RZSM predictions more closely align with both the spatially comprehensive, but temporally infrequent, L2/3 RZSM data, and the temporally resolved, but spatially restricted, observations at most of the sites, preserving the inter-daily variability that cannot be provided by L2/3 RZSM (purple lines in Figure 2). Compared to the native ED2 and L2/3 RZSM, the blended results L2/3 RZSM-B have higher r values (0.69 and 0.72 for the results in the 0–10 and 10–40 cm of soil layers, sample size $n_{2/3} = 101$) and lower RMSDs (0.081 and 0.067 for the results in the two soil layers) relative to the observations (Text S1 and Figure S2). The site-level correlation coefficients, RMSDs, and bias values of L2/3 RZSM-B compared to the in situ observations (sample sizes given by the value of n_{obs} in each panel of Figure 2) are given in Table S3. While simple, this blending approach provided an effective way to continuously update and reduce the bias in the ED2 soil moisture predictions using the infrequent L2/3 RZSM observations.

To further assess the effectiveness of the blending method, we also applied our interpolation and bias correction to the time points in the in situ soil moisture observations that correspond to the AirMOSS L2/3

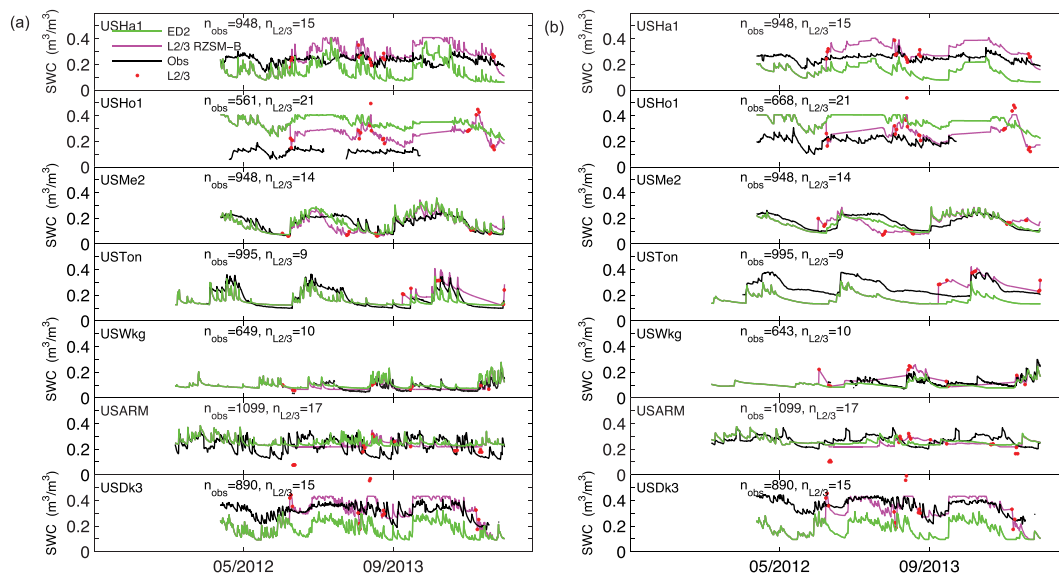


Figure 2. Comparison of daily soil water content (θ in units of m^3/m^3) predicted by ED2 terrestrial biosphere model (green lines) against in situ ground-based measurements (black lines) and AirMOSS L2/3 measurements (red dots) at the seven flux tower sites. Panel (a) the 0- to 10-cm soil layer and panel (b) the 10- to 40-cm soil layer. The magenta lines in each panel show the blended L2/3 RZSM-B time series produced by the bias reduction procedure described in section 2.3. The number of records for the in situ observations and AirMOSS L2/3 measurements are also shown in the figure.

snapshots to produce a blended ED2 RZSM series for the flux tower sites. As illustrated in Figure S3, this time series more closely matches the observational time series (RZSM biases decrease from -0.01 ± 0.10 to $0.00 \pm 0.04 \text{ m}^3/\text{m}^3$ and RMSEs decrease from 0.10 ± 0.06 to $0.07 \pm 0.03 \text{ m}^3/\text{m}^3$), confirming that the linear blending method is effective in reducing the biases in the model's soil moisture predictions.

Both the native ED2-RZSM and radar-constrained L2/3 RZSM-B show clear spatial gradients across the seven regions (Figures 3a and 3b). Not surprisingly, eastern regions like Duke Forest and Howland Forest have higher annual mean RZSM than the drier western regions like Walnut Gulch and MOISST (Figure 3b).

However, ED2 RZSM predictions are surprisingly low at Harvard Forest that also has a wet climate while the radar-constrained RZSM implies much higher RZSM in this region (compare Figures 3a and 3b). In addition, the L2/3 RZSM-B shows surprisingly high values in Howland (Figure 3b). Comparison of L2/3 RZSM and L2/3 RZSM-B against the ground observations at Howland (Figure 2) indicates that the AirMOSS L2/3 RZSM measurements (red points) used to produce the L2/3 RZSM-B (purple line) are generally lower than the ground measurements on the corresponding dates (Figure 2). The reason(s) for this large discrepancy between AirMOSS-derived estimates and ground-based RZSM measurements at Howland is unclear: It may due to error in AirMOSS RZSM retrieval algorithm and/or errors in the Howland ground-based measurements whose values are notably lower than the ground-based measurements at the Harvard Forest, another northeastern forest site. The radar-constrained L2/3 RZSM-B shows high values in Tonzi Ranch, which has a relatively dry climate (Figure 3b). In part this reflects the fact that most of the Tonzi Ranch flights occurred in the wet season as indicated by the red dots shown in Figure 2. Some of these high values are confirmed by the corresponding ground observations at the USTon flux tower site (Figure 2).

As shown in Figure 3c, ED2's RZSM predictions are lower than L2/3 RZSM-B in 86.9% of the combined area of the seven study regions, implying that the ED2 model has a general tendency to underestimate RZSM relative to both the *in-situ* observations and SAR-retrieved RZSM estimates. Exceptions include a western portion of Metolius and a northern portion of MOISST that have a wet biases (Figure 3c). The region with the smallest overall bias is Metolius with a near-zero regional average bias ($0.003 \text{ m}^3/\text{m}^3$; Figure 3c), while the regional largest biases are at the two northeastern forest regions (Howland and Harvard) with regional average biases of 0.21 and $0.19 \text{ m}^3/\text{m}^3$, respectively (Figure 3c). The distribution of mean biases (relative to AirMOSS L2/3 RZSM) over the AirMOSS observing period (September 2012 to August 2014) in three soil layers (0–10, 10–40, and 40–100 cm) in the ED2 model across the study regions confirms the above

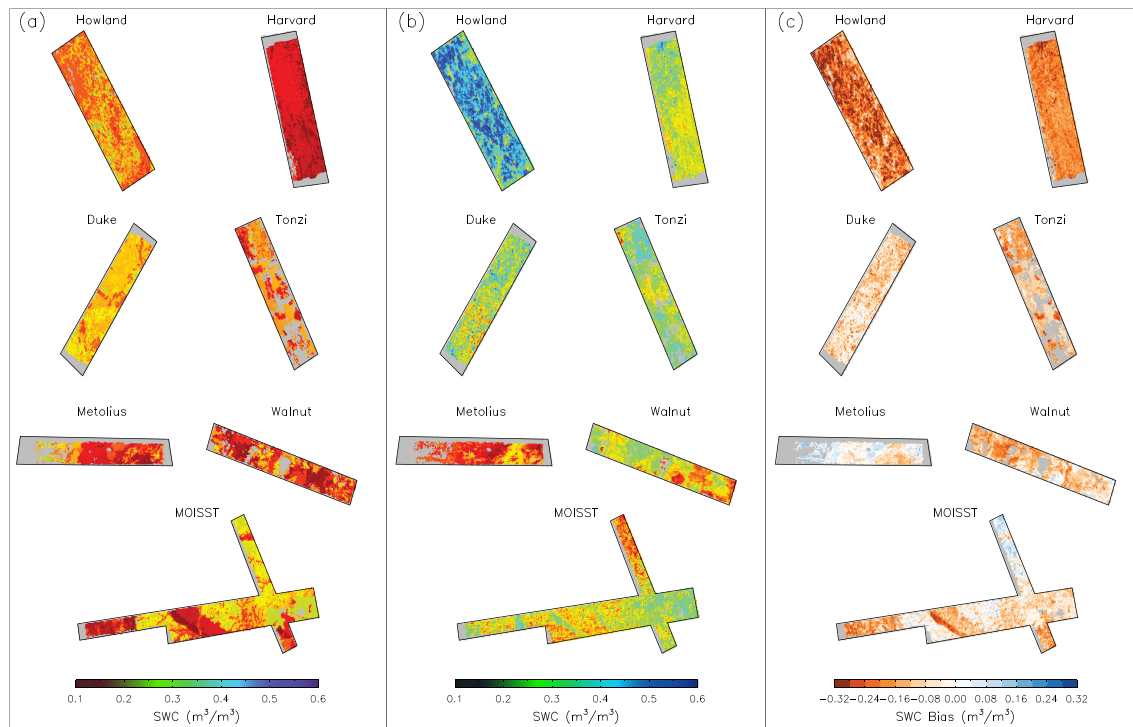


Figure 3. Panels a and b: spatial patterns of mean RZSM (θ in units of m^3/m^3) during the AirMOSS observation period (September 2012 to August 2014) in the 0- to 100-cm soil layers in the seven evaluation areas for (a) original ED2 simulations corresponding to the AirMOSS flights; (b) the AirMOSS L2/3 data. Panel (c): estimated mean biases in the model's predictions (ED2 minus L2/3 RZSM-B). The number of AirMOSS snapshots during the 2012–2014 observation period are: 21, 15, 15, 9, 14, 10, and 17 for Howland, Harvard, Duke, Tonzi, Metolius, Walnut, and MOISST, respectively.

findings: In all regions except for Metolius, the average regional soil moisture biases are generally negative ranging from 0.05 to $-0.22 \text{ m}^3/\text{m}^3$ (see Figure 3c, Text S2, and Figure S4). There is also a trend towards increasing levels of bias in deeper soil layers (Figure S4) suggesting that ED2 RZSM dry bias may be primarily caused by excessive drainage rather than excessive evapotranspiration.

The model's dry-bias tendency is also apparent in the simulations at five of seven flux tower sites, the two exceptions being the Howland (USHo1) and Metolius (USMe2) flux towers (Figure 2). A multiple linear regression of spatial RZSM biases on the potential controlling factors suggest that the RZSM biases covary significantly with soil texture (sand and clay percentage), as well as with AGB and PFTs, but not with LAI (Table S4), a pattern that is also consistent with idea that the model's dry bias is caused by moisture drainage occurring too quickly within the model's the soil column.

4.2. Comparison of Spatiotemporal Patterns of Carbon Fluxes from Native ED2 Simulations and ED2 L2/3 RZSM-B Simulations

Figure 4a shows the spatial patterns of annual GPP in the seven regions predicted by the original ED2 simulations (i.e. native rather than bias-corrected soil moisture). Harvard Forest, Howland Forest, Duke Forest, and western Metolius have higher GPP values, with respective regional means of 1.09, 1.33, 1.14, and $1.23 \text{ kg}\cdot\text{cm}^{-2}\cdot\text{year}^{-1}$, than the other regions (eastern Metolius, Tonzi Ranch, MOISST, and Walnut Gulch), with regional means of 0.31, 0.27, 0.23, and $0.06 \text{ kg}\cdot\text{cm}^{-2}\cdot\text{year}^{-1}$, respectively (Figure 4a). Compared to the original ED2 predictions, GPP in the ED2 + L2/3 RZSM-B (i.e. with bias corrected soil moisture) is generally higher in all the evaluation regions except for Metolius (compare Figures 4a and 4b). Regional average annual GPP values for Harvard Forest, Howland Forest, Duke Forest, Metolius, Tonzi Ranch, MOISST, and Walnut Gulch are, respectively, 1.89, 1.50, 2.15, 1.01, 0.27, 0.27, and $0.47 \text{ kg}\cdot\text{cm}^{-2}\cdot\text{year}^{-1}$, that is, the RZSM correction alters annual GPP by 73.4%, 13.5%, 88.5%, -28.3% , 3.7%, 17.4%, and 683% in the seven regions. As would be expected given the general dry bias in the native ED2 model, the differences in GPP are almost all positive: the only exception is at Metolius where ED2 + L2/3

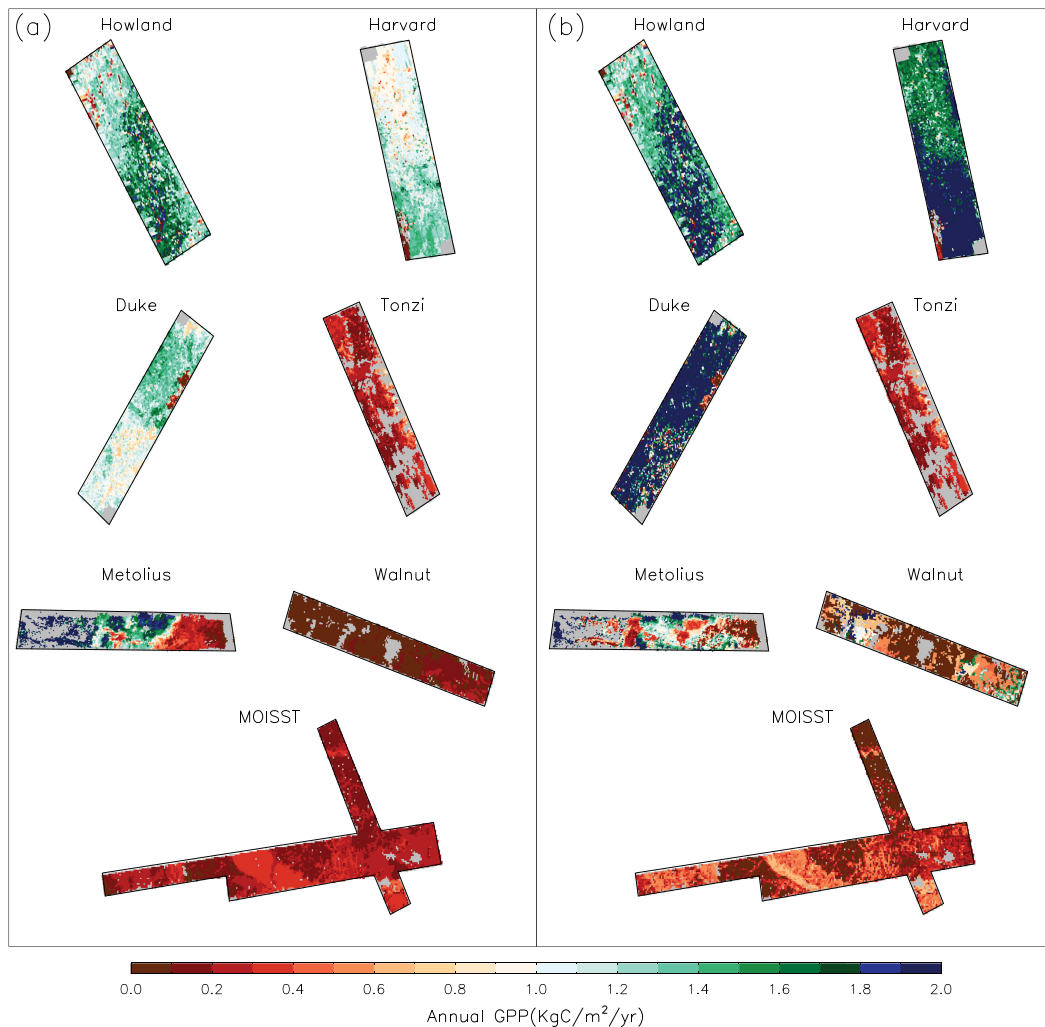


Figure 4. Maps of annual GPP in the seven regions: the results from original ED2 simulations (a) and ED2 simulations driven by L2/3 RZSM-B (b).

RZSM-B's GPP is lower in some regions of eastern and central Metolius (compare Figures 4a and 4b) where original ED2 RZSM had a wet bias (see Figure 3c). As might be expected given the large dry biases between original ED2 RZSM and L2/3 RZSM-B seen at Harvard and Howland (see Figure 3c), the increases in GPP at both these sites are relatively large; however, large changes also occurred at Duke Forest and Walnut Gulch (Figure 4, compare panels a and b) where the magnitude of the dry biases were lower.

RZSM correction also causes changes in ecosystem respiration. At Harvard Forest and Howland Forest, where the RZSM biases in the ED2 simulations were larger (Figure 3c), both R_a and R_h (Figures S5 and S6) increase significantly once the RZSM moisture biases are reduced. The impacts of RZSM corrections on R_a ranged in magnitude from 0.05 to 0.30 $\text{kg}\cdot\text{cm}^{-2}\cdot\text{year}^{-1}$ and, not surprisingly, are strongly correlated with the changes in GPP (compare Figures S5 and 4). The responses of R_h to soil moisture corrections were generally larger than those of R_a , ranging from 0.60 to 0.84 $\text{kg}\cdot\text{cm}^{-2}\cdot\text{year}^{-1}$. Although the RZSM bias at Duke Forest was smaller than at Harvard Forest and Howland Forest (Figure 3c), the changes in R_a and R_h at Duke Forest resulting from RZSM correction were both large (Figures S5 and S6). For the regions with smaller biases in modeled RZSM (Tonzi, MOISST, and Walnut), RZSM bias reduction has modest impacts on the two respiration terms: Changes of annual values are within $\pm 0.100 \text{ kg}\cdot\text{cm}^{-2}\cdot\text{year}^{-1}$ (Figures S5 and S6).

Since NEE is the difference between ecosystem respiration and GPP, the effects of soil moisture on NEE depend on the relative magnitudes and directions of how soil moisture affects ecosystem respiration and GPP. As seen in Figures S5 and S6, across the Howland Forest and Harvard Forest evaluation regions, the

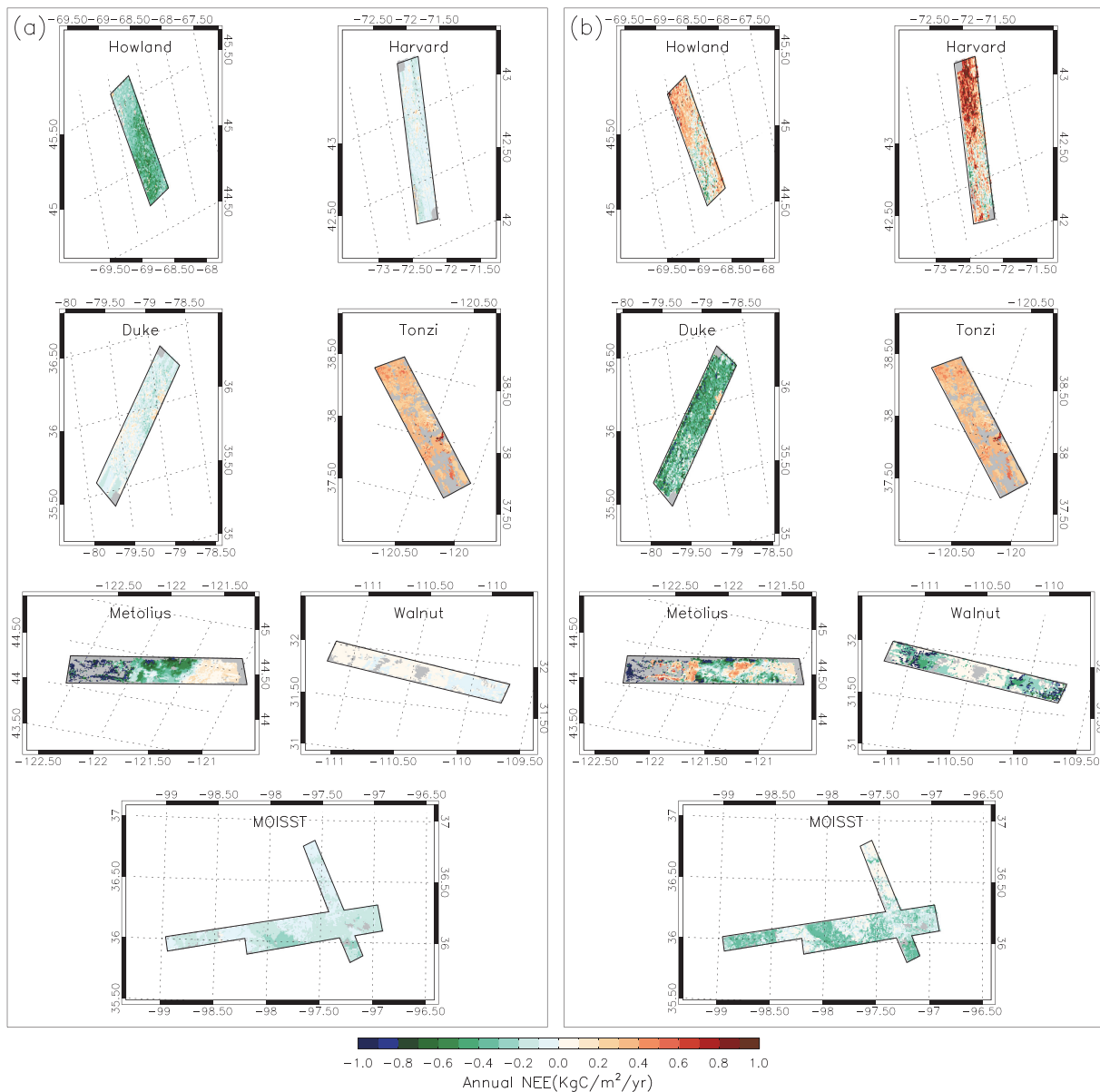


Figure 5. Maps of annual net ecosystem exchange (NEE) in the seven regions. (a) the results from native ED2 simulations; and (b) ED2 simulations incorporating L2/3 RZSM-B moisture product.

correction of the general dry bias in RZSM ed to increases of R_a and R_h . Because the increases in GPP arising from the moisture bias reduction (Figure 4) are smaller than the combined increases in R_a and R_h following the moisture bias reduction (Figures S5 and S6), regional average NEE increases by $0.37\text{--}0.47\text{ kg}\cdot\text{cm}^{-2}\cdot\text{year}^{-1}$ in these two regions (Figure 5). At Metolius, after correcting RZSM, annual NEE across most of the region also increases (Figure 5); however, in this case the increased NEE is largely due to reductions in GPP following bias reduction (Figure 4), as these areas have wet biases in the model (Figure 3c). In contrast, NEE across the Duke Forest, Walnut Gulch, and MOISST regions decrease (become more negative) following soil moisture correction (Figure 5), decreasing regional average NEE by $0.04\text{--}0.31\text{ kg}\cdot\text{cm}^{-2}\cdot\text{year}^{-1}$. At Tonzi, changes in annual NEE are minimal (Figure 5) because the impacts of RZSM bias correction on GPP (Figure 4) and ecosystem respiration ($R_a + R_h$, Figures S5 and S6) are small, and are of similar magnitude and thus approximately cancel each other out.

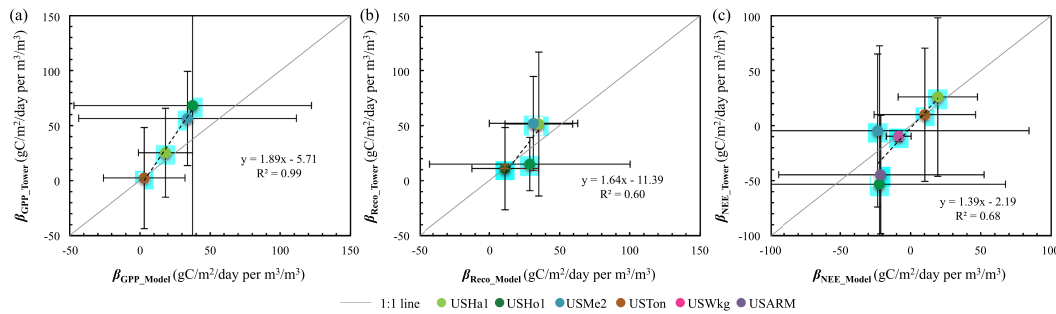


Figure 6. Comparison of the ED2 and tower observation-based daily carbon flux sensitivities (β_{GPP} , β_{ECO} , and β_{NEE} , equation (1)) from 2010 to 2014 at the Harvard (USHa1), Howland (USHo1), Metolius (USMe2), Tonzi (USTon), Walnut Gulch (USWkg), and MOISST (USARM) flux towers (a) β_{GPP} , (b) β_{ECO} , and (c) β_{NEE} ; closed circles indicate the sample means, while both horizontal and vertical bars denote the standard deviations of the samples.

4.3. Evaluation of Modeled Carbon Flux Sensitivities to Soil Moisture

The ED2 daily C-flux sensitivities (β_{GPP} , β_{ECO} , and β_{NEE}) agree reasonably well with the observation-based C-flux sensitivity estimates as indicated by high r values ($r > 0.77$, $P < 0.001$; Figure 6). The model's predictions of β_{GPP} match the observations better than its predictions of β_{ECO} and β_{NEE} : the model explains 99% of the variability in observation-based β_{GPP} estimates (Figure 6a), while its predictions of β_{ECO} and β_{NEE} explain 60% and 68% of the observation-based estimates, respectively (Figures 6b and 6c). While it is clear that there are large day-to-day variabilities in both model- and observation-based C-flux sensitivities, as indicated by the vertical and horizontal error bars in Figure 6, the signs and magnitudes of the model's predicted sensitivities align with the observation-based site-level means distributed along the 1:1 lines (Figure 6). However, the ED2 model tends to underestimate the sensitivities of GPP and ecosystem respiration to RZSM (biases of -14.89 ± 14.35 and -5.60 ± 15.76 g C/m³/day per m³/m³ for β_{GPP} and β_{ECO} , respectively). Consequently, the mean bias in ED2 β_{NEE} tends to be overestimated (5.12 ± 18.75 g C/m³/day per m³/m³).

4.4. Spatial Patterns of Carbon Flux Sensitivities to Soil Moisture

To better understand the carbon cycle implications of spatial and temporal variation in soil moisture, we used equation (1) to quantify the relative sensitivities of GPP, R_a , and R_h to changes in RZSM. As shown in Figure 7, 95.5%, 90.9%, and 94.3% of the seven regions have positive values for β_{GPP} , β_{Ra} , and β_{Rh} , respectively, indicating that increased RZSM generally enhances vegetation productivity, autotrophic respiration, and heterotrophic respiration.

The magnitudes of β_{GPP} , β_{Ra} , and β_{Rh} exhibit large spatial variability between regions. β_{GPP} and β_{Ra} are the highest in Duke Forest and in most areas of Metolius; values are also high in the northwest and southeast portions of Walnut Gulch, Harvard Forest, and central portions of Tonzi Ranch (Figures 7a and 7b). The lowest values in absolute magnitude are found in northern Howland Forest and most areas of MOISST (Figures 7a and 7b). It is also notable that there are also some areas with negative β_{GPP} , β_{Ra} , and β_{Rh} values, which are mainly located in the central portions of the Metolius and Walnut regions (Figures 7a–7c). Regional average β_{GPP} is higher in Duke Forest, Metolius, and Harvard Forest and lower values in Walnut Gulch, Tonzi Ranch, MOISST, and Howland Forest (Table 3). Regional average values of β_{Ra} in the seven regions range between 0.4 and 9.8 kg·cm⁻²·year⁻¹· θ^{-1} . In other words, a region-wide increase of 0.01 m³/m³ in RZSM (θ) across the seven regions can alter regional average vegetation productivity by 0.016–0.19 kg·cm⁻²·year⁻¹· θ^{-1} (i.e., 16–190 t C km⁻²·year⁻¹) and regional average vegetation respiration by 0.004–0.098 kg·cm⁻²·year⁻¹· θ^{-1} (i.e., 4–98 t C km⁻²·year⁻¹). In contrast, β_{Rh} shows different spatial pattern across the regions with the highest values in the eastern regions of Harvard Forest, Duke Forest, and Howland Forest and lower values in the three western regions and the central regions (Figure 7c; Table 3).

Because NEE is a net difference between ecosystem respiration (R_a plus R_h) and GPP, the sign of its sensitivity to RZSM can be either positive or negative, depending on sign and magnitude of changes in ecosystem respiration and GPP. In most areas of Harvard and Howland Forest, 42.9% of Tonzi Ranch, and 39.4% of Walnut Gulch, β_{NEE} is positive, indicating that increased RZSM leads to reduced carbon gain in these regions (Figure 8). In contrast, β_{NEE} is negative across most of the Duke, Metolius, and MOIST regions and over the

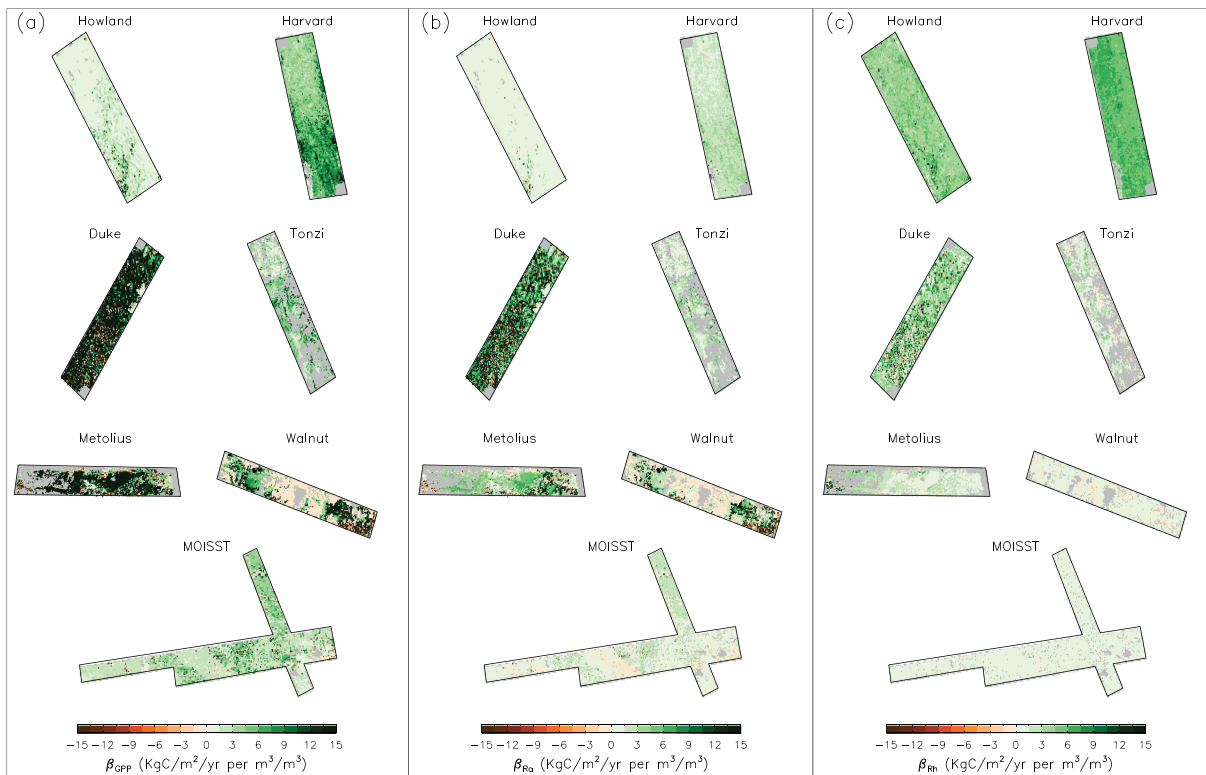


Figure 7. Spatial patterns of yearly carbon flux sensitivities (β_{GPP} , β_{Ra} , and β_{Rh} equation (1)) in the seven evaluation regions (a) β_{GPP} , (b) β_{Ra} , and (c) β_{Rh} .

remaining portions of Tonzi Ranch and Walnut Gulch, indicating that increased RZSM in these areas increases carbon storage (Figure 8).

4.5. Causes of Spatial Variation in Carbon Flux Sensitivities

To understand the underlying causes of the spatial variability in carbon flux sensitivities, we conducted a multiple linear regression to relate the spatial values of carbon flux sensitivity with the corresponding spatial values of AGB, LAI, soil carbon, soil texture, and dominant PFT type. The multiple linear regression results show that, of the canopy structure and soil attribute metrics examined, the strongest determinants (as measured by the magnitude of the standardized regression coefficients, B , Table 4) of the GPP and autotrophic respiration moisture sensitivities (β_{GPP} and β_{Ra}) are canopy LAI and soil clay fraction (both positive effects, i.e., increased sensitivity) and AGB (negative effect, i.e., reduced sensitivity). In contrast, the strongest determinant of the heterotrophic moisture sensitivity (β_{Rh}) is soil carbon content (positive effect). The above effects reflect themselves in the moisture sensitivity of β_{NEE} , which varies positively with AGB (and to a lesser extent soil carbon), and negatively with LAI and clay fraction (Table 4).

The carbon flux sensitivity metrics also vary with canopy composition (Table 4). In particular, both β_{GPP} and β_{Ra} covary strongly and positively with mid-successional hardwood, fir, southern pine, and western pine

Table 3
Summary of Regional C-flux Sensitivity Metrics and Their Spatial Variabilities (Standard Deviations).

Variables	Harvard Forest	Howland Forest	Duke Forest	Metolius	Walnut Gulch	Tonzi Ranch	MOISST
β_{GPP} ($\text{kg}\cdot\text{cm}^{-2}\cdot\text{year}^{-1}\cdot\theta^{-1}$)	6.0 ± 3.4	1.6 ± 3.0	18.9 ± 35.9	12.7 ± 17.9	4.2 ± 36.7	4.1 ± 3.6	2.8 ± 3.0
β_{Ra} ($\text{kg}\cdot\text{cm}^{-2}\cdot\text{year}^{-1}\cdot\theta^{-1}$)	2.2 ± 1.2	0.4 ± 1.1	9.8 ± 19.4	4.1 ± 8.1	1.7 ± 14.3	2.1 ± 1.9	0.6 ± 1.2
β_{Rh} ($\text{kg}\cdot\text{cm}^{-2}\cdot\text{year}^{-1}\cdot\theta^{-1}$)	5.7 ± 0.9	4.2 ± 1.5	4.2 ± 4.6	1.9 ± 2.8	0.2 ± 0.3	1.3 ± 1.3	0.2 ± 0.1
β_{NEE} ($\text{kg}\cdot\text{cm}^{-2}\cdot\text{year}^{-1}\cdot\theta^{-1}$)	2.0 ± 2.6	3.1 ± 1.9	-5.0 ± 13.3	-6.7 ± 12.1	-2.3 ± 22.3	-0.8 ± 2.6	-2.0 ± 1.9

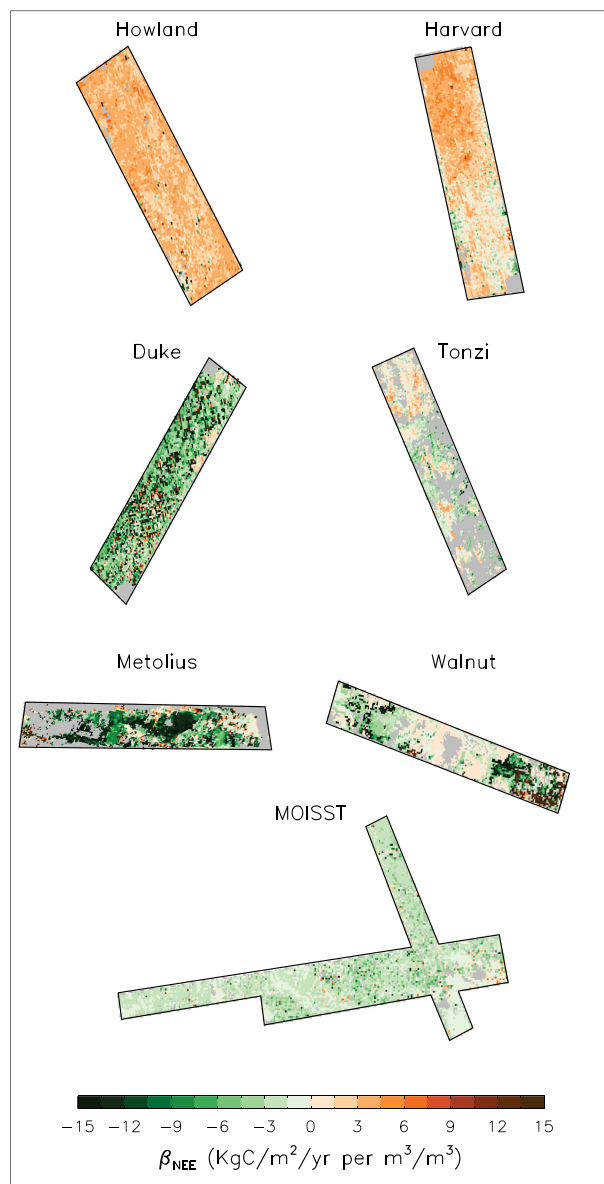


Figure 8. Spatial patterns of the sensitivity of yearly net ecosystem exchange (NEE) to variation in soil moisture (β_{NEE} , equation (1)).

while ecosystems dominated by late conifer, C_3 crop, early-successional hardwood, western hardwood, and late-successional hardwoods exhibit the lowest sensitivities (Figure 9a). β_{Ra} shows similar patterns of sensitivity (Figure 9b).

Regarding the sensitivity of soil decomposition (R_h) to RZSM, mid-successional hardwood, southern pine, late conifer, and late-successional hardwood ecosystems show the highest sensitivities, followed by western pine, fir, western hardwood, and dryland C_3 grass, while early-successional hardwood ecosystems, dryland C_4 grass, and C_3 crop exhibit the lowest sensitivities (Figure 9c). Further discussion of these patterns, along with an analysis of the seasonal patterns of carbon flux sensitivities, can be found in Text S3.

These differences in carbon sensitivities explain the spatial patterns of β_{GPP} , β_{Ra} , β_{Rh} , and β_{NEE} seen in Figures 7 and 8. The Duke Forest region is mainly composed of middle-successional hardwoods and southern pines; the Harvard Forest region is largely composed of middle-successional hardwoods; the dominant PFTs in the Metolius region are fir and western pines (Table 1). All of the above PFTs show high

canopy fractions, and negatively with late conifer and late-successional hardwood canopy fractions. With respect to compositional influences on heterotrophic respiration, β_{Rh} covaries strongly and positively with southern pine, mid-successional hardwood, late conifer, and late-successional hardwood canopy fractions and negatively with dryland C_3 grass and fir canopy fractions (Table 4). These composition effects reflect themselves in the moisture sensitivity of β_{NEE} (Table 4), which varies positively with late conifer and late-successional hardwood canopy fractions (reflecting their negative effects on β_{GPP} and positive effects on β_{Rh}) and negatively with dryland C_3 grass, fir, and western pine canopy fractions (reflecting the positive effect of western pines and fir fractions on β_{GPP} , and the negative effects of western pines, fir, and dryland C_3 grass fractions on β_{Rh}).

Some of these results relationships are intuitive: For example, LAI directly affects canopy-scale photosynthetic capacity and thus can directly impact GPP. Similarly, clay fraction affects moisture drainage and thus directly impacts soil hydrological processes implemented in the model, and soil carbon determines the size of the belowground carbon pool available for heterotrophic respiration. However, other effects, such as the negative relationships between AGB and GPP and between AGB and R_a , and the effects of PFT are less intuitive, likely reflecting indirect effects on the carbon flux sensitivities.

Many parameters governing photosynthesis and autotrophic respiration vary between PFTs (Alton, 2011; Lawrence et al., 2011). In addition, although heterotrophic respiration is not directly affected by PFT type, the different PFTs have differential rates leaf turnover, root turnover, and mortality that influence the supply of carbon for heterotrophic respiration. The different PFTs also have different lignin to nitrogen ratios and different rates of water uptake that can indirectly affect decomposition rates by influencing levels of soil moisture. Accordingly, we explored whether the differential sensitivities of GPP, R_a , and R_h seen within and between regions were linked to differences in PFT composition of the ecosystem.

We investigated the differential ecological sensitivities of different PFTs to RZSM through an ANOVA analysis and a comparison of the C-flux sensitivity distributions among different PFTs (Figure 9). As figure illustrates, the different PFTs show different sensitivities to RZSM changes. Southern pine, fir, and mid-successional hardwood dominated ecosystems exhibit the highest sensitivities of GPP and R_a to RZSM, followed by dryland C_3 grass, western pine, and dryland C_4 grass-dominated ecosystems,

Table 4

Summary of the Multiple Linear Regression Analyses of the Four Annual C-flux Sensitivity Metrics on AGB, LAI, Soil Carbon Storage, Sand Percentage, Clay Percentage, and Plant Functional Type (A Categorical Variable with C₃ Crop as Default Type) Across the Study Regions

Explanatory variables	Carbon flux sensitivity											
	β_{GPP}			β_{Ra}			β_{Rh}			β_{NEE}		
	<i>B</i>	<i>P</i>	Sig.	<i>B</i>	<i>P</i>	Sig.	<i>B</i>	<i>P</i>	Sig.	<i>B</i>	<i>P</i>	Sig.
(Constant)	−0.51	<0.001	***	−0.63	<0.001	***	−0.78	<0.001	***	−0.04	<0.001	***
Canopy structure												
AGB	−0.52	<0.001	***	−0.61	<0.001	***	0.02	0.25	n.s.	0.41	<0.001	***
LAI	0.38	<0.001	***	0.46	<0.001	***	0.11	<0.001	***	−0.21	<0.001	***
Soil attributes												
Soil carbon	0.15	<0.001	***	0.15	<0.001	***	0.46	<0.001	***	0.10	<0.001	***
Sand percentage	0.17	<0.001	***	0.15	<0.001	***	0.06	<0.001	***	−0.16	<0.001	***
Clay percentage	0.50	<0.001	***	0.48	<0.001	***	−0.04	<0.001	***	−0.51	<0.001	***
Plant functional types												
Dryland C ₃ grass	0.27	<0.001	***	0.13	<0.03	*	−0.88	<0.001	***	−0.51	<0.001	***
Dryland C ₄ grass	0.20	<0.001	***	0.30	<0.001	***	0.13	<0.001	***	−0.02	0.50	n.s.
Early Hardwood	0.07	0.31	n.s.	0.17	<0.001	***	0.20	<0.001	***	0.14	0.01	*
Fir	1.18	<0.001	***	1.05	<0.001	***	−0.70	<0.001	***	−1.62	<0.001	***
Late conifer	−0.28	<0.001	***	−0.12	0.01	*	0.53	<0.001	***	0.68	<0.001	***
Late hardwood	−0.28	<0.001	***	−0.16	0.03	*	0.43	<0.001	***	0.61	<0.001	***
Middle hardwood	1.02	<0.001	***	1.16	<0.001	***	1.32	<0.001	***	−0.15	<0.001	***
Southern pine	0.78	<0.001	***	0.84	<0.001	***	1.40	<0.001	***	0.04	0.54	n.s.
Western hardwood	0.38	<0.01	***	0.63	<0.001	***	−0.26	0.02	*	−0.25	0.05	*
Western pine	0.64	<0.001	***	0.75	<0.001	***	−0.27	<0.001	***	−0.64	<0.001	***

Note. Regression coefficients (*B*) are standardized.

sensitivities of GPP and R_a to increased RZSM, indicated by the generally high β_{GPP} and β_{Ra} values across these regions. In contrast, the Howland Forest region is dominated by late-successional conifer ecosystems, and the MOISST region is mainly composed of C₃ crop and dryland C₄ grass ecosystems (Table 1). As seen in Figures 9a and 9b, the late-successional conifer, C₃ crop, and dryland C₄ grass dominated ecosystems have relatively low sensitivities of GPP and R_a to increases in soil moisture, which explains the lower β_{GPP} and β_{Ra} values found across the Howland Forest and MOISST regions (Figure 7). Similarly, the high sensitivity of heterotrophic respiration (R_h) to increases in soil moisture in mid-successional hardwood and late-successional conifer dominated ecosystems (Figure 9c) explains the high values of β_{Rh} found across the Harvard Forest and Howland Forest regions (Figure 7).

Soil texture is another potentially important factor underlying the spatial variation in carbon flux sensitivities. We investigated this by examining the sensitivities of modeled RZSM (0–100 cm), GPP, R_{eco} , and NEE to soil texture at the seven flux tower sites. The results for the Harvard Forest flux tower (USHa1) site show how RZSM increases with increasing clay percentage and decreases with increasing sand percentage (Figure 10a). Similar patterns are seen the other six sites (Figure S7). GPP has the opposite response to increasing clay percentage and increasing sand percentage (compare Figures 10a and 10b). The effects of soil texture on GPP at the other six sites are also generally similar to those seen at the Harvard Flux tower (Figure S8). In contrast, R_{eco} generally increases as sand percentage rises while the relationship between R_{eco} and clay percentage is a non-monotonic, U-shaped function (Figures 10c and S9).

These effects of soil texture on GPP and R_{eco} give rise to the following relationships between NEE and soil texture. At all sites, NEE declines with increasing sand content, but the degree of sensitivity varies: Harvard exhibits high sensitivity to changes in sand percentage (Figure 10d), as do the Howland, Tonzi, Metolius, and MOIST flux tower sites (Figure S10a,c,d,f, respectively), while the Duke and Walnut Gulch flux tower sites exhibit low sensitivity to changes in sand content (Figure S10b,e, respectively). With respect to clay content, NEE generally increases with increasing clay content with a similar pattern of sensitivity to that seen for sand, that is, high sensitivity at Harvard (Figure 10d), and similarly at Howland, Tonzi, Metolius, and MOIST (Figure S10a,c,d, f, respectively), and low sensitivities at the Duke and Walnut Gulch flux tower sites.

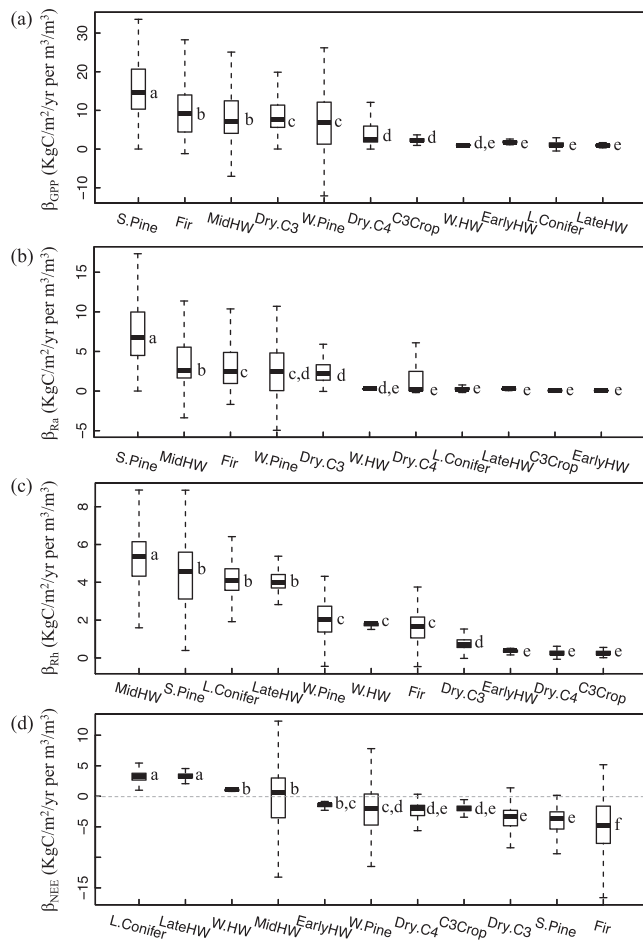


Figure 9. Boxplots of yearly carbon flux sensitivities, (a) β_{GPP} , (b) β_{RA} , (c) β_{RH} , and (d) β_{NEE} , across dominant plant functional types; the means of the boxplots with the same letters are not significantly different (ANOVA test, $P > 0.001$).

5. Discussion

In this study, we used newly available radar-derived estimates of RZSM across seven representative regions in North America to (1) evaluate the accuracy of terrestrial biosphere model predictions of soil moisture dynamics and to (2) quantify the sensitivity of terrestrial carbon fluxes to spatial and temporal variation in soil moisture. To our knowledge, this is the first study to systematically assess the accuracy of terrestrial biosphere model predictions of spatio-temporal variability in RZSM and its impact on terrestrial carbon fluxes across the major biomes of North America. The results have several important implications for earth system modeling, terrestrial ecology, and hydrology communities.

5.1. Importance of Regional High-Quality Soil Data and Pedotransfer Functions

In site-level simulations driven by observed soil information and meteorological forcing, overall negative biases appear in predictions of RZSM at four out of seven sites (Figure 2). A similar result was found in the regional simulations: RZSM via the ED2 biosphere model also had an overall dry bias of $-0.07 \text{ m}^3/\text{m}^3$ (Figures 3 and S4). The highest levels of bias were in the northeastern temperate broad-leaved and mixed forest biomes, where the average levels of bias in these two regions were 0.19 and $0.21 \text{ m}^3/\text{m}^3$, respectively.

The dry bias in ED2 model's soil moisture predictions likely reflects errors in the model's soil hydrology formulation. Our sensitivity analyses clearly demonstrate that the hydrological and carbon dynamics implemented in the ED2 model are sensitive to soil texture and associated soil physical parameters (see Table 4, Figures 10 and S7–S10). As in many terrestrial biosphere and land-surface models, ED2 uses a Richards equation formulation (Richards, 1931). The key parameters of this formulation are the hydraulic conductivity function $K(\theta)$, which determines the rate of vertical movement of moisture in the soil as a function of its wetness (θ), and the saturated and residual soil water contents (θ_s and θ_{\min}), which respectively determine the upper and lower physical bounds of soil water content.

Like many terrestrial biosphere and land surface models, in ED2 these soil parameters are calculated using the Clapp and Hornberger (1978) pedotransfer functions, which specify the values for these parameters based on the percentages of sand, clay, and silt in the soil.

The calibration and parameterization of pedotransfer functions largely depend on the size and representativeness of training samples (Borgesen et al., 2008) and sample dimension (Ghanbarian et al., 2017), making it hard to develop universally-applicable pedotransfer functions for all biomes investigated in this study. An important next step will be to evaluate alternate pedotransfer functions such as the Van Genuchten (1980) soil hydraulic functions. Analysis has shown that the Van Genuchten (1980) pedotransfer functions are more accurate than Clapp and Hornberger (1978) pedotransfer functions (Shao & Irannejad 1999). More recently, some researchers (Nemes et al., 2006; Patil & Chaturvedi, 2012) have advocated the use of non-parametric nearest-neighbor models as an alternative to conventional parametric formulations such as Clapp and Hornberger (1978) and Van Genuchten (1980), and the development of an improved set of pedotransfer functions (Patil & Singh, 2016). It may also be necessary to incorporate region-specific values for soil properties, which can be determined from advanced statistical or intelligence techniques (Merdun, 2010), rather than applying a universal parametric pedotransfer function.

Uncertainty in soil texture measurements can also introduce errors into soil moisture simulations. Although gSSURGO is arguably the best available soil database across the United States (Zhong & Xu, 2011) the accuracy of this database varies across regions and depends on the spatial scale over which it is implemented (Drohan et al., 2003; Mednick, 2010). A cross-validation of the gSSURGO data set by Ramcharan et al. (2018)

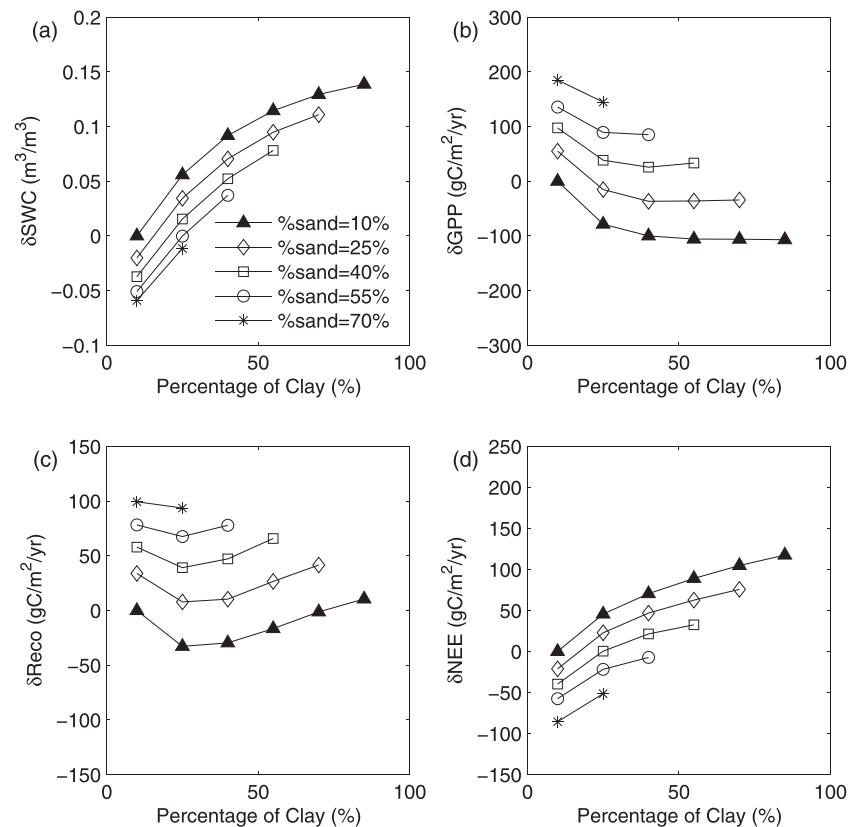


Figure 10. Sensitivities of ED2 (a) soil water content (0–100 cm), (b) GPP, (c) ecosystem respiration, and (d) NEE to sand and clay fractions at the Harvard Forest (USHa1) flux tower site under the average climatic condition between 2010 and 2014; all values are normalized by the modeled value with sand percentage = 10% and clay percentage = 10%.

showed that RMSE for percent sand and clay are about 17.8% and 12%, respectively. For example, according to our sensitivity analyses (Figures 10a and S7), this level of uncertainty in percent sand (clay) would introduce $8 \pm 2\%$ ($9 \pm 14\%$) uncertainty in the ED2 regional RZSM. In the regional model simulations, errors in RZSM may also reflect errors in the NLDAS meteorological forcing data set (Nearing et al., 2016; Xia et al., 2016). However, errors in climatological forcing are unlikely to be the primary cause of the inaccuracies in RZSM prediction because, as seen in Figure 2, errors of similar magnitude to those seen in the regional simulations also arose in the simulations at the flux tower sites that used observed meteorological forcing data.

Our intercomparison of ED2, AirMOSS L2/3, and L2/3 blended RZSM show that the RMSE of AirMOSS L2/3 is about $0.08\text{--}0.099 \text{ m}^3/\text{m}^3$ (Figures 2 and S2), which is consistent with the result of a previous study (Tabatabaenejad et al., 2015). These errors in the AirMOSS L2/3 data set in turn affect the blended RZSM (Figure 2). Although our simple RZSM blending method utilizes the radar-based AirMOSS L2/3 product to improve the predictions of RZSM, the algorithm does not explicitly consider the uncertainty and error in the data source (i.e., the AirMOSS L2/3 RZSM in this study). An important avenue for future studies will be to propagate the error and uncertainty from the AirMOSS data into the model's soil moisture state variables and examine its consequences for resulting carbon fluxes and carbon flux sensitivities. In particular, the penetration depth of the P-band SAR instrument varies across landscapes and depends on soil wetness, soil type, and vegetation type. As noted by Tabatabaenejad et al. (2015), these uncertainties introduce error in the SAR-based RZSM estimates for the 0- to 100-cm soil layer. Further studies on the spatial variability of penetration depth of the P-band SAR will be important for further improving the accuracy of RZSM measurements.

In addition, the current aircraft platform of the P-band SAR instrument means that the frequency of the AirMOSS RZSM measurements is relatively low, providing measurements only a few times per year.

Consequently, as seen in Figure 2, the accuracy of the blended RZSM estimates vary significantly as function of time since the last RZSM measurement. An important future step will be to examine the trade-off between temporal revisit frequency and spatial resolution of RZSM measurements that could be obtained from a satellite deployment of the P-band SAR instrument to constrain and improve terrestrial biosphere model predictions of soil moisture and resulting carbon fluxes.

5.2. Impacts of Soil Moisture on Terrestrial Carbon Fluxes

Our analysis shows that uncertainty and inaccuracies in RZSM can have large impacts on the estimates of terrestrial carbon fluxes (Figures 4, 5, S5, and S6). A change in RZSM by $0.01 \text{ m}^3/\text{m}^3$ can lead to changes in GPP, R_a , and R_h across the major biomes in North America by 0.016–0.189, 0.004–0.098, and 0.002–0.057 $\text{kg}\cdot\text{cm}^{-2}\cdot\text{year}^{-1}\cdot\theta^{-1}$, respectively. The response of NEE to change of RZSM is more complicated since it depends on the relative impacts of soil moisture on GPP, R_a , and R_h (ranging between -6.99 and $3.11 \text{ kg}\cdot\text{cm}^{-2}\cdot\text{year}^{-1}\cdot\theta^{-1}$). As the positive β_{NEE} values indicate, the analysis shows that increases in soil moisture do not necessarily increase net carbon storage: For example, increases in RZSM in most areas of Harvard and Howland Forest regions decrease net carbon storage (i.e., increased NEE) by 2.0 and $3.1 \text{ kg}\cdot\text{cm}^{-2}\cdot\text{year}^{-1}\cdot\theta^{-1}$, respectively (Figure 8) because increased RZSM (ΔRZSM) induced increases of ecosystem respiration are considerably larger than ΔRZSM -induced increases in GPP (Figures 7 and 8) in these two areas. This is likely because the low RZSM values predicted across the Harvard and Howland Forest regions (Figure 3a) inhibit ecosystem respiration in these regions. When the dry biases in RZSM are corrected, it causes marked increases in ecosystem respiration. In contrast, increases of RZSM in most areas of the other five regions increased estimates of net carbon storage with values ranging between -6.69 and $-0.76 \text{ kg}\cdot\text{cm}^{-2}\cdot\text{year}^{-1}\cdot\theta^{-1}$ (Figure 8).

Errors in modeled RZSM impact not only estimates of carbon fluxes but also estimates of water and energy fluxes. Previous studies through site-level observations and modeling have shown that hydrological processes and surface energy partitioning are strongly sensitive to RZSM (Berg et al., 2014; Crow & Ryu, 2009; Gallego-Elvira et al., 2016). Model parameters controlling the calculation of RZSM are critical for accurate prediction of RZSM and corresponding carbon flux calculation. For example Dietze et al. (2014) conducted a synthesis of carbon cycle uncertainties in the ED2 model using the Predictive Ecosystem Analyzer eco-informatics workflow. They found that uncertainty of water conductance parameter in the ED2 model was generally high across PFTs due to a lack of direct measurements and suggested that adding even small amounts of data constraints is likely to be effective in reducing this predictive uncertainty. Since carbon, water, and energy fluxes of ecosystems are inherently coupled, inaccuracies and uncertainties of RZSM can also introduce significant error into the predictions of terrestrial water and energy fluxes (Exbrayat et al., 2013; Falloon et al., 2011; Gallego-Elvira et al., 2016).

ESMs Terrestrial biosphere models are often calibrated using past observations of carbon fluxes. However, structural errors and uncertainty in soil parameterization can introduce considerable uncertainty for future projections (Falloon et al., 2011) because future climate conditions are expected to be out of the current and past norms. Improving the soil hydrology models and pedotransfer functions of ESMs and biosphere models may not, by itself, improve accuracy in their carbon flux predictions. The interactions of between soil hydrology, plant carbon fluxes, and soil decomposition mean that errors in hydrology tend to result in knock-on errors or distortions in other model components such as photosynthesis and surface energy schemes that have been tuned (either intentionally or unintentionally) to compensate for errors in predicting soil moisture.

Accumulation of errors in soil moisture dynamics and carbon fluxes is also likely to significantly impact long-term vegetation dynamics in terrestrial biosphere models. For example, in the ED2 model, soil moisture is an important environmental variable controlling the phenology of drought-deciduous PFTs. With regard to long-term dynamics, changes in soil moisture impact plant growth, mortality and reproduction through its impacts on plant productivity and respiration that affect these demographic processes by influencing the plant's net carbon balance. Finally, while correcting soil moisture in the model can improve near-term predictions, improved long-term predictions of future carbon and vegetation dynamics (for example, in response to climate change) will require improvements in the underlying representation of soil physics.

5.3. Differential Sensitivities of North American Ecosystems to Variation in RZSM

Our results indicate that North American ecosystems dominated by different PFTs exhibit markedly different responses and sensitivities to changes in RZSM (Figure 9): Middle-successional hardwood, southern pine, and fir-dominated ecosystems generally show the large sensitivities to RZSM, grassland ecosystems generally show intermediate sensitivities, while early hardwood and late conifer-dominated ecosystems have the lowest sensitivities to RZSM (Figure 9). The different carbon flux components of the same PFT show different sensitivities to RZSM. In particular, the Harvard Forest and Duke Forest regions (both dominated by middle-successional hardwoods, Table 1) and the Metolius region (dominated by fir and western pine, Table 1) exhibit higher levels of carbon flux sensitivities than the other regions (Figures 7 and 8). These differential sensitivities may reflect differences in underlying plant traits, which in the terrestrial biosphere model are reflected in the parameter values of the PFTs. Many of these parameters are specified from plant trait databases or previous field and experimental studies (Longo, 2014; Medvigy et al., 2009; Moorcroft et al., 2001); however, other plant parameters, such as those determining aboveground and belowground carbon allocation, are less well-constrained introducing uncertainty in the estimated carbon sensitivities. The differences may also reflect correlated differences in climate regimes and soil hydraulic properties between the different ecosystem types. Likely correlated with the differing responses of carbon fluxes to variation in RZSM are differing levels of ecosystem resilience to climate-change introduced droughts. Ensuring that terrestrial biosphere models can correctly capture the responses of North American ecosystems to changes in RZSM is an important step to improving projections of how the composition and structure of terrestrial ecosystems will change as a result of climate-driven changes in moisture regimes. Accounting for divergent responses of different ecosystems within ESMs and biosphere models is also critical for accurately modeling carbon cycles (Frasson et al., 2015) and for projecting ecosystem responses and carbon-climate feedbacks to future climate change (Alton, 2011; Pendall et al., 2011; K Zhang et al., 2015).

Acknowledgments

This research was funded by National Aeronautical and Space Administration grant (NASA EarthVenture-1 09-EV109-0006) to M.M. with a sub-contract to P.M. at Harvard University, and National Natural Science Foundation of China (51879067), Natural Science Foundation of Jiangsu Province (BK20180022) and Six Talent Peaks Project in Jiangsu Province (NY-004) grants to K.Z. Part of the research was carried out at the Jet Propulsion Laboratory, California Institute of Technology, under a contract with the National Aeronautics and Space Administration. The AirMOSS L2 hourly in-ground soil moisture observations are available from https://daac.ornl.gov/AIRMOSS/guides/AirMOSS_L2_Inground_Soil_Moist.html. The AirMOSS L2/3 volumetric soil moisture profiles data are available from <https://doi.org/10.3334/ORNLDAAC/1418>. The carbon flux data at the seven flux tower sites are available from <https://ameriflux.lbl.gov>. The SSURGO data are from <https://websoilsurvey.nrcs.usda.gov/>. The data sets produced as part of this study are available from the Oak Ridge National Laboratory Distributed Active Archive Center (ORNL-DAAC): <https://doi.org/10.3334/ORNLDAAC/1422>. The NLCD 2011 data are from <https://www.mrlc.gov/data/nlcd-2011-land-cover-conus>. The MODIS Global Land Cover Dynamics Product is from <https://e4ftl01.cr.usgs.gov/MOTA/>. The source codes of ED2 model are available from <https://github.com/EDmodel/ED2>.

6. Conclusions

In this study, newly-available remote sensing derived measurements of RZSM were incorporated into a terrestrial biosphere model to investigate the significance of spatial and temporal variation in RZSM for predictions of terrestrial carbon fluxes across the major ecosystems of North America. The analysis indicates that (i) the terrestrial biosphere model exhibits significant biases in its predictions of RZSM; and (ii) the responses of terrestrial carbon fluxes to spatial and temporal variation in soil moisture exhibit complex patterns due to its differential impacts on carbon uptake (gross primary productivity) and carbon losses (plant and soil respiration). The results highlight the marked differences in the sensitivity of terrestrial carbon fluxes in different ecosystems to changes in RZSM and the need for additional work to understand the underlying causes of these ecosystem differences. Understanding how changes in soil moisture impact predictions of long-term as well as short-term carbon fluxes also needs to be investigated.

References

- Albani, M., Medvigy, D., Hurtt, G. C., & Moorcroft, P. R. (2006). The contributions of land-use change, CO₂ fertilization, and climate variability to the Eastern US carbon sink. *Global Change Biology*, 12(12), 2370–2390. <https://doi.org/10.1111/j.1365-2486.2006.01254.x>
- Alton, P. B. (2011). How useful are plant functional types in global simulations of the carbon, water, and energy cycles? *Journal of Geophysical Research*, 116, G01030. <https://doi.org/10.1029/2010JG001430>
- Baldocchi, D. D., Xu, L. K., & Kiang, N. (2004). How plant functional-type, weather, seasonal drought, and soil physical properties alter water and energy fluxes of an oak-grass savanna and an annual grassland. *Agricultural and Forest Meteorology*, 123(1–2), 13–39. <https://doi.org/10.1016/j.agrformet.2003.11.006>
- Berg, A., Lintner, B. R., Findell, K. L., Malyshev, S., Loikith, P. C., & Gentile, P. (2014). Impact of soil moisture-atmosphere interactions on surface temperature distribution. *Journal of Climate*, 27(21), 7976–7993.
- Borgesen, C. D., Iversen, B. V., Jacobsen, O. H., & Schaap, M. G. (2008). Pedotransfer functions estimating soil hydraulic properties using different soil parameters. *Hydrological Processes*, 22(11), 1630–1639.
- Camps, A., Park, H., Pablos, M., Foti, G., Gommenginger, C. P., Liu, P., & Judge, J. (2016). Sensitivity of GNSS-R spaceborne observations to soil moisture and vegetation. *IEEE J-Stars*, 9(10), 4730–4742. <https://doi.org/10.1109/JSTARS.2016.2588467>
- Chapin, E., A. Chau, J. Chen, B. Heavey, S. Hensley, Y. Lou, et al. (2012). AirMOSS: An airborne P-band SAR to measure root zone soil moisture, in *Proceedings of Radar Conference 2012*, edited, p. 6, Atlanta, GA.
- Clapp, R. B., & Hornberger, G. M. (1978). Empirical equations for some soil hydraulic-properties. *Water Resources Research*, 14(4), 601–604.
- Crow, W. T., & Ryu, D. (2009). A new data assimilation approach for improving runoff prediction using remotely-sensed soil moisture retrievals. *Hydrology and Earth System Sciences*, 13(1), 1–16.
- Dietze, M. C., Serbin, S. P., Davidson, C., Desai, A. R., Feng, X., Kelly, R., et al. (2014). A quantitative assessment of a terrestrial biosphere model's data needs across North American biomes. *Journal of Geophysical Research: Biogeosciences*, 119, 286–300. <https://doi.org/10.1002/2013JG002392>

- Dorigo, W. A., Wagner, W., Hohensinn, R., Hahn, S., Paulik, C., Xaver, A., et al. (2011). The International Soil Moisture Network: A data hosting facility for global in situ soil moisture measurements. *Hydrology and Earth System Sciences*, 15(5), 1675–1698.
- Drohan, P. J., Ciolkosz, E. J., & Petersen, G. W. (2003). Soil survey mapping unit accuracy in forested field plots in northern Pennsylvania. *Soil Science Society of America Journal*, 67(1), 208–214.
- Entekhabi, D., Njoku, E. G., O'Neill, P. E., Kellogg, K. H., Crow, W. T., Edelstein, W. N., et al. (2010). The Soil Moisture Active Passive (SMAP) mission. *Proceedings of the IEEE*, 98(5), 704–716. <https://doi.org/10.1109/Jproc.2010.2043918>
- Exbrayat, J. F., Pitman, A. J., Zhang, Q., Abramowitz, G., & Wang, Y. P. (2013). Examining soil carbon uncertainty in a global model: Response of microbial decomposition to temperature, moisture and nutrient limitation. *Biogeosciences*, 10(11), 7095–7108.
- Falloon, P., Jones, C. D., Ades, M., & Paul, K. (2011). Direct soil moisture controls of future global soil carbon changes: An important source of uncertainty. *Global Biogeochemical Cycles*, 25, GB3010. <https://doi.org/10.1029/2010GB003938>
- Flanagan, L. B., & Johnson, B. G. (2005). Interacting effects of temperature, soil moisture and plant biomass production on ecosystem respiration in a northern temperate grassland. *Agricultural and Forest Meteorology*, 130(3–4), 237–253.
- Ford, T. W., Quiring, S. M., Frauenfeld, O. W., & Rapp, A. D. (2015). Synoptic conditions related to soil moisture-atmosphere interactions and unorganized convection in Oklahoma. *Journal of Geophysical Research: Atmospheres*, 120, 11,519–11,535. <https://doi.org/10.1002/2015JD023975>
- Frasson, R. P. D., Bohrer, G., Medvigy, D., Matheny, A. M., Morin, T. H., Vogel, C. S., et al. (2015). Modeling forest carbon cycle response to tree mortality: Effects of plant functional type and disturbance intensity. *Journal of Geophysical Research: Biogeosciences*, 120, 2178–2193. <https://doi.org/10.1002/2015JG003035>
- Friedlingstein, P., Cox, P., Betts, R., Bopp, L., von Bloh, W., Brovkin, V., et al. (2006). Climate-carbon cycle feedback analysis: Results from the C(4)MIP model intercomparison. *Journal of Climate*, 19(14), 3337–3353.
- Gallego-Elvira, B., Taylor, C. M., Harris, P. P., Ghent, D., Veal, K. L., & Folwell, S. S. (2016). Global observational diagnosis of soil moisture control on the land surface energy balance. *Geophysical Research Letters*, 43, 2623–2631. <https://doi.org/10.1002/2016GL068178>
- Ganguly, S., Friedl, M. A., Tan, B., Zhang, X. Y., & Verma, M. (2010). Land surface phenology from MODIS: Characterization of the Collection 5 global land cover dynamics product. *Remote Sensing of Environment*, 114(8), 1805–1816.
- Gelman, A., & Rubin, D. B. (1992). Inference from iterative simulation using multiple sequences. *Statistical Science*, 7, 457–472.
- Ghanbarian, B., Taslimitehrani, V., & Pachepsky, Y. A. (2017). Accuracy of sample dimension-dependent pedotransfer functions in estimation of soil saturated hydraulic conductivity. *Catena*, 149, 374–380.
- Gumuzzio, A., Brocca, L., Sanchez, N., Gonzalez-Zamora, A., & Martinez-Fernandez, J. (2016). Comparison of SMOS, modelled and in situ long-term soil moisture series in the northwest of Spain. *Hydrological Sciences Journal-Journal Des Sciences Hydrologiques*, 61(14), 2610–2625.
- He, M. Z., Kimball, J. S., Running, S., Ballantyne, A., Guan, K. Y., & Huemmrich, F. (2016). Satellite detection of soil moisture related water stress impacts on ecosystem productivity using the MODIS-based photochemical reflectance index. *Remote Sensing of Environment*, 186, 173–183.
- Hollinger, D. Y., Aber, J., Dail, B., Davidson, E. A., Goltz, S. M., Hughes, H., et al. (2004). Spatial and temporal variability in forest-atmosphere CO₂ exchange. *Global Change Biology*, 10(10), 1689–1706. <https://doi.org/10.1111/j.1365-2486.2004.00847.x>
- Homer, C. G., Dewitz, J. A., Yang, L., Jin, S., Danielson, P., Xian, G., et al. (2015). Completion of the National Land Cover Database for the conterminous United States-representing a decade of land cover change information Photogramm. *Eng. Remote. Sens.*, 81, 345–354.
- Huang, Y. Y., Gerber, S., Huang, T. Y., & Lichstein, J. W. (2016). Evaluating the drought response of CMIP5 models using global gross primary productivity, leaf area, precipitation, and soil moisture data. *Global Biogeochemical Cycles*, 30, 1827–1846. <https://doi.org/10.1002/2016GB005480>
- Hursh, A., Ballantyne, A., Cooper, L., Maneta, M., Kimball, J., & Watts, J. (2017). The sensitivity of soil respiration to soil temperature, moisture, and carbon supply at the global scale. *Global Change Biology*, 23(5), 2090–2103.
- Hurt, G. C., Dubayah, R., Drake, J., Moorcroft, P. R., Pacala, S. W., Blair, J. B., & Fearon, M. G. (2004). Beyond potential vegetation: Combining lidar data and a height-structured model for carbon studies. *Ecological Applications*, 14(3), 873–883. <https://doi.org/10.1890/02-5317>
- Hurt, G. C., Moorcroft, P. R., Pacala, S. W., & Levin, S. A. (1998). Terrestrial models and global change: challenges for the future. *Global Change Biology*, 4(5), 581–590. <https://doi.org/10.1046/j.1365-2486.1998.t01-1-00203.x>
- Ito, D., & Ishida, S. (2016). Short- and long-term effects of soil moisture on soil respiration in an apple orchard. *Journal of Agricultural Meteorology*, 72(2), 63–71.
- Jia, X., Zha, T. S., Gong, J. N., Wang, B., Zhang, Y. Q., Wu, B., et al. (2016). Carbon and water exchange over a temperate semi-arid shrubland during three years of contrasting precipitation and soil moisture patterns. *Agricultural and Forest Meteorology*, 228, 120–129.
- Juszk, I., Eugster, W., Heijmans, M. M. P. D., & Schaepman-Strub, G. (2016). Contrasting radiation and soil heat fluxes in Arctic shrub and wet sedge tundra. *Biogeosciences*, 13(13), 4049–4064.
- Kerr, Y. H., Waldteufel, P., Richaume, P., Wigneron, J. P., Ferrazzoli, P., Mahmoodi, A., et al. (2012). The SMOS soil moisture retrieval algorithm. *IEEE Transactions on Geoscience and Remote Sensing*, 50(5), 1384–1403.
- Kim, H., & Lakshmi, V. (2018). Use of Cyclone Global Navigation Satellite System (CyGNSS) observations for estimation of soil moisture. *Geophysical Research Letters*, 45, 8272–8282. <https://doi.org/10.1029/2018GL078923>
- Kim, Y., Moorcroft, P. R., Aleinov, I., Puma, M. J., & Kiang, N. Y. (2015). Variability of phenology and fluxes of water and carbon with observed and simulated soil moisture in the Ent Terrestrial Biosphere Model (Ent TBM version 1.0.1.0.0). *Geoscientific Model Development*, 8(12), 3837–3865. <https://doi.org/10.5194/gmd-8-3837-2015>
- Knox, R. (2012). Land conversion in Amazonia and northern South America: Influences on regional hydrology and ecosystem response, Massachusetts Institute of Technology.
- Knox, R. G., Longo, M., Swann, A. L. S., Zhang, K., Levine, N. M., Moorcroft, P. R., & Bras, R. L. (2015). Hydrometeorological effects of historical land-conversion in an ecosystem-atmosphere model of Northern South America. *Hydrology and Earth System Sciences*, 19(1), 241–273. <https://doi.org/10.5194/hess-19-241-2015>
- Koster, R. D., Guo, Z. C., Yang, R. Q., Dirmeyer, P. A., Mitchell, K., & Puma, M. J. (2009). On the nature of soil moisture in land surface models. *Journal of Climate*, 22(16), 4322–4335. <https://doi.org/10.1175/2009jcli2832.1>
- Lawrence, D. M., Oleson, K. W., Flanner, M. G., Thornton, P. E., Swenson, S. C., Lawrence, P. J., et al. (2011). Parameterization improvements and functional and structural advances in version 4 of the community land model. *Journal of Advances in Modeling Earth Systems*, 3, M03001. <https://doi.org/10.1029/2011MS00045>

- Levine, N. M., Zhang, K., Longo, M., Baccini, A., Phillips, O. L., Lewis, S. L., et al. (2016). Ecosystem heterogeneity determines the ecological resilience of the Amazon to climate change. *Proceedings of the National Academy of Sciences of the United States of America*, 113(3), 793–797.
- Lin, T. S., & Cheng, F. Y. (2016). Impact of soil moisture initialization and soil texture on simulated land-atmosphere interaction in Taiwan. *Journal of Hydrometeorology*, 17(5), 1337–1355.
- Lindell, D. B., & Long, D. G. (2016). High-resolution soil moisture retrieval with ASCAT. *IEEE Geoscience and Remote Sensing Society*, 13(7), 972–976.
- Liu, S. L., Roujean, J. L., Tchuente, A. T. K., Ceamanos, X., & Calvet, J. C. (2014). A parameterization of SEVIRI and MODIS daily surface albedo with soil moisture: Calibration and validation over southwestern France. *Remote Sensing of Environment*, 144, 137–151.
- Loew, A., Stacked, T., Dorigo, W., de Jeu, R., & Hagemann, S. (2013). Potential and limitations of multidecadal satellite soil moisture observations for selected climate model evaluation studies. *Hydrology and Earth System Sciences*, 17(9), 3523–3542.
- Lokupitiya, E., Denning, S., Paustian, K., Baker, I., Schaefer, K., Verma, S., et al. (2009). Incorporation of crop phenology in simple biosphere model (SiBcrop) to improve land-atmosphere carbon exchanges from croplands. *Biogeosciences*, 6(6), 969–986.
- Longo, M. (2014). *Amazon forest response to changes in rainfall regime: Results from an individual-based dynamic vegetation model*, (p. 311). Cambridge, Massachusetts: Harvard University.
- McInerney, E., & Helton, A. M. (2016). The effects of soil moisture and emergent herbaceous vegetation on carbon emissions from constructed wetlands. *Wetlands*, 36(2), 275–284. <https://doi.org/10.1007/s13157-016-0736-9>
- McRoberts, R. E., Bechtold, W. A., Patterson, P. L., Scott, C. T., Reams, G. A. (2005). The enhanced forest inventory and analysis program of the USDA forest service: historical perspective and announcements of statistical documentation. *Journal of Forestry*, 3(6), 304–308.
- Mednick, A. C. (2010). Does soil data resolution matter? State Soil Geographic Database versus Soil Survey Geographic Database in rainfall-runoff modeling across Wisconsin. *Journal of Soil and Water Conservation*, 65(3), 190–199.
- Medvigy, D., & Moorcroft, P. R. (2012). Predicting ecosystem dynamics at regional scales: an evaluation of a terrestrial biosphere model for the forests of northeastern North America. *Philosophical Transactions of the Royal Society Series B*, 367, 222–235.
- Medvigy, D., Wofsy, S. C., Munger, J. W., Hollinger, D. Y., & Moorcroft, P. R. (2009). Mechanistic scaling of ecosystem function and dynamics in space and time: Ecosystem demography model version 2. *Journal of Geophysical Research*, 114, G01002. <https://doi.org/10.1029/2008JG000812>
- Merdun, H. (2010). Alternative methods in the development of pedotransfer functions for soil hydraulic characteristics. *Eurasian Soil Science*, 43(1), 62–71.
- Moorcroft, P. R., Hurtt, G. C., & Pacala, S. W. (2001). A method for scaling vegetation dynamics: The ecosystem demography model (ED). *Ecological Monographs*, 71(4), 557–585.
- Morbidelli, R., Saltalippi, C., Flammini, A., Corradini, C., Brocca, L., & Govindaraju, R. S. (2016). An investigation of the effects of spatial heterogeneity of initial soil moisture content on surface runoff simulation at a small watershed scale. *Journal of Hydrology*, 539, 589–598.
- Nearing, G. S., Mocko, D. M., Peters-Lidard, C. D., Kumar, S. V., & Xia, Y. L. (2016). Benchmarking NLDAS-2 soil moisture and evapotranspiration to separate uncertainty contributions. *Journal of Hydrometeorology*, 17(3), 745–759.
- Nemes, A., Rawls, W. J., & Pachepsky, Y. A. (2006). Use of the nonparametric nearest neighbor approach to estimate soil hydraulic properties. *Soil Science Society of America Journal*, 70(2), 327–336. <https://doi.org/10.2136/sssaj2005.0128>
- Njoku, E. G., Jackson, T. J., Lakshmi, V., Chan, T. K., & Nghiem, S. V. (2003). Soil moisture retrieval from AMSR-E. *IEEE Transactions on Geoscience and Remote Sensing*, 41(2), 215–229.
- Palmroth, S., Maier, C. A., McCarthy, H. R., Oishi, A. C., Kim, H. S., Johnsen, K. H., et al. (2005). Contrasting responses to drought of forest floor CO₂ efflux in a Loblolly pine plantation and a nearby Oak-Hickory forest. *Global Change Biology*, 11(3), 421–434. <https://doi.org/10.1111/j.1365-2486.2005.00915.x>
- Paloscia, S., Macelloni, G., Santi, E., & Koike, T. (2001). A multifrequency algorithm for the retrieval of soil moisture on a large scale using microwave data from SMMR and SSM/I satellites. *IEEE Transactions on Geoscience and Remote Sensing*, 39(8), 1655–1661.
- Pan, M., Cai, X. T., Chaney, N. W., Entekhabi, D., & Wood, E. F. (2016). An initial assessment of SMAP soil moisture retrievals using high-resolution model simulations and in situ observations. *Geophysical Research Letters*, 43, 9662–9668. <https://doi.org/10.1002/2016gl069964>
- Parinussa, R. M., Holmes, T. R. H., Wanders, N., Dorigo, W. A., & de Jeu, R. A. M. (2015). A preliminary study toward consistent soil moisture from AMSR2. *Journal of Hydrometeorology*, 16(2), 932–947.
- Parinussa, R. M., Wang, G., Holmes, T. R. H., Liu, Y. Y., Dolman, A. J., de Jeu, R. A. M., et al. (2014). Global surface soil moisture from the microwave radiation imager onboard the Fengyun-3B satellite. *International Journal of Remote Sensing*, 35(19), 7007–7029.
- Patil, N. G., & Chaturvedi, A. (2012). Pedotransfer functions based on nearest neighbour and neural networks approach to estimate available water capacity of shrink-swell soils. *Indian Journal of Agricultural Sciences*, 82(1), 35–38.
- Patil, N. G., & Singh, S. K. (2016). Pedotransfer functions for estimating soil hydraulic properties: A review. *Pedosphere*, 26(4), 417–430.
- Pendall, E., Osanai, Y., Williams, A. L., & Hovenden, M. J. (2011). Soil carbon storage under simulated climate change is mediated by plant functional type. *Global Change Biology*, 17(1), 505–514.
- Polcher, J., Piles, M., Gelati, E., Barella-Ortiz, A., & Tello, M. (2016). Comparing surface-soil moisture from the SMOS mission and the ORCHIDEE land-surface model over the Iberian Peninsula. *Remote Sensing of Environment*, 174, 69–81.
- Ramcharan, A., Hengl, T., Nauman, T. W., Brungard, C. W., Waltman, S., Wills, S., & Thompson, J. (2018). Soil property and class maps of the conterminous United States at 100-meter spatial resolution. *Soil Science Society of America Journal*, 82(1), 186–201. <https://doi.org/10.2136/sssaj2017.04.0122>
- Richards, L. A. (1931). Capillary conduction of liquids through porous mediums. *Physics*, 1(5), 318–333. <https://doi.org/10.1063/1.1745010>
- Scott, R. L. (2010). Using watershed water balance to evaluate the accuracy of eddy covariance evaporation measurements for three semiarid ecosystems. *Agricultural and Forest Meteorology*, 150(2), 219–225. <https://doi.org/10.1016/j.agrformet.2009.11.002>
- Shaw, J. D. (2009). Using FIA data in the Forest Vegetation Simulator. In W. McWilliams, G. Moisen, R. Czaplewski, (Eds.), comps. Forest Inventory and Analysis (FIA) Symposium 2008; October 21–23, 2008; Park City, UT. Proc. RMRS-P-56CD. Fort Collins, CO: U.S. Department of Agriculture, Forest Service, Rocky Mountain Research Station. 16 p.
- Shao, Y., & Irannejad, P. (1999). On the Choice of Soil Hydraulic Models in Land-Surface Schemes Boundary-Layer. *Meteorology*, 90, 83–115.
- Song, C. Y., & Jia, L. (2016). A method for downscaling Fengyun-3B soil moisture based on apparent thermal inertia. *Remote Sensing*, 8(9).
- Suarez, A., Mahmood, R., Quintanar, A. I., Beltran-Przekurat, A., & Pielke, R. (2014). A comparison of the MM5 and the regional atmospheric modeling system simulations for land-atmosphere interactions under varying soil moisture. *Tellus Series a-Dynamic Meteorology and Oceanography*, 66, 21486. <https://doi.org/10.3402/tellusa.v66.21486>

- Sugathan, N., Biju, V., & Renuka, G. (2014). Influence of soil moisture content on surface albedo and soil thermal parameters at a tropical station. *Journal of Earth System Science*, 123(5), 1115–1128.
- Tabatabaeenejad, A., Burgin, M., Duan, X. Y., & Moghaddam, M. (2015). P-band radar retrieval of subsurface soil moisture profile as a second-order polynomial: First AirMOSS results. *IEEE Transactions on Geoscience and Remote Sensing*, 53(2), 645–658. <https://doi.org/10.1109/Tgrs.2014.2326839>
- Thomas, C. K., Law, B. E., Irvine, J., Martin, J. G., Pettijohn, J. C., & Davis, K. J. (2009). Seasonal hydrology explains interannual and seasonal variation in carbon and water exchange in a semiarid mature ponderosa pine forest in central Oregon. *Journal of Geophysical Research*, 114, G04006. <https://doi.org/10.1029/2009JG001010>
- Truong-Loi, M. L., Saatchi, S., & Jaruwatanadilok, S. (2015). Soil moisture estimation under tropical forests using UHF radar polarimetry. *IEEE Transactions on Geoscience and Remote Sensing*, 53(4), 1718–1727. <https://doi.org/10.1109/Tgrs.2014.2346656>
- Urbanski, S., Barford, C., Wofsy, S., Kucharik, C., Pyle, E., Budney, J., et al. (2007). Factors controlling CO₂ exchange on timescales from hourly to decadal at Harvard Forest. *Journal of Geophysical Research*, 112, G02020. <https://doi.org/10.1029/2006JG000293>
- van den Hurk, B., Kim, H., Krinner, G., Seneviratne, S. I., Derksen, C., Oki, T., et al. (2016). LS3MIP (v1.0) contribution to CMIP6: The land surface, snow and soil moisture model intercomparison project—Aims, setup and expected outcome. *Geoscientific Model Development*, 9(8), 2809–2832.
- Van Genuchten, M. T. (1980). A closed-form equation for predicting the hydraulic conductivity of unsaturated soils. *Soil Science Society of America Journal*, 44(5), 892–898.
- Verrot, L., & Destouni, G. (2016). Data-model comparison of temporal variability in long-term time series of large-scale soil moisture. *Journal of Geophysical Research: Atmospheres*, 121, 10,056–10,073. <https://doi.org/10.1002/2016JD025209>
- Wagner, W., Lemoine, G., & Rott, H. (1999). A method for estimating soil moisture from ERS scatterometer and soil data. *Remote Sensing of Environment*, 70(2), 191–207. [https://doi.org/10.1016/S0034-4257\(99\)00036-X](https://doi.org/10.1016/S0034-4257(99)00036-X)
- Walker, J. P., & Houser, P. R. (2004). Requirements of a global near-surface soil moisture satellite mission: accuracy, repeat time, and spatial resolution. *Advances in Water Resources*, 27(8), 785–801.
- Walko, R. L., Band, L. E., Baron, J., Kittel, T. G., Lammers, R., Lee, T. J., et al. (2000). Coupled atmosphere-biophysics-hydrology models for environmental modeling. *Journal of Applied Meteorology*, 39(6), 931–944.
- Xia, J. B., Zhao, Z. G., Sun, J. K., Liu, J. T., & Zhao, Y. Y. (2017). Response of stem sap flow and leaf photosynthesis in *Tamarix chinensis* to soil moisture in the Yellow River Delta, China. *Photosynthetica*, 55(2), 368–377.
- Xia, Y. L., Cosgrove, B. A., Mitchell, K. E., Peters-Lidard, C. D., Ek, M. B., Kumar, S., et al. (2016). Basin-scale assessment of the land surface energy budget in the national centers for environmental prediction operational and research NLDAS-2 systems. *Journal of Geophysical Research: Atmospheres*, 121, 196–220. <https://doi.org/10.1002/2015JD023889>
- Xia, Y. L., Mitchell, K., Ek, M., Sheffield, J., Cosgrove, B., Wood, E., et al. (2012). Continental-scale water and energy flux analysis and validation for the North American Land Data Assimilation System project phase 2 (NLDAS-2): 1. Intercomparison and application of model products. *Journal of Geophysical Research*, 117, D03109. <https://doi.org/10.1029/2011JD016048>
- Xia, Y. L., Sheffield, J., Ek, M. B., Dong, J. R., Chaney, N., Wei, H. L., et al. (2014). Evaluation of multi-model simulated soil moisture in NLDAS-2. *Journal of Hydrology*, 512, 107–125.
- Xu, L. K., Baldocchi, D. D., & Tang, J. W. (2004). How soil moisture, rain pulses, and growth alter the response of ecosystem respiration to temperature. *Global Biogeochemical Cycles*, 18, GB4002. <https://doi.org/10.1029/2004GB002281>
- Xu, Z. Z., & Zhou, G. S. (2005). Effects of soil moisture on gas exchange, partitioning of fed (CO₂)-C-14 and stable carbon isotope composition (δ C-13) of *Leymus chinensis* under two different diurnal temperature variations. *Journal of Agronomy and Crop Science*, 191(1), 27–34.
- Yan, K., Park, T., Yan, G., Chen, C., Yang, B., Liu, Z., et al. (2016). Evaluation of MODIS LAI/FPAR Product Collection 6. Part 1: Consistency and Improvements. *Remote Sensing*, 8, 359. <https://doi.org/10.3390/rs8050359>
- Zhang, K., de Almeida Castanho, A. D., Galbraith, D. R., Moghim, S., Levine, N. M., Bras, R. L., et al. (2015). The fate of Amazonian ecosystems over the coming century arising from changes in climate, atmospheric CO₂ and land-use. *Global Change Biology*, 21(7), 2569–2587. <https://doi.org/10.1111/gcb.12903>
- Zhang, Y. F., Wang, X. P., Hu, R., Pan, Y. X., & Zhang, H. (2014). Variation of albedo to soil moisture for sand dunes and biological soil crusts in arid desert ecosystems. *Environment and Earth Science*, 71(3), 1281–1288.
- Zhong, B., & Xu, Y. J. (2011). Scale effects of geographical soil datasets on soil carbon estimation in Louisiana, USA: A comparison of STATSGO and SSURGO. *Pedosphere*, 21(4), 491–501.